Schwebel, Alan H.

CARBON DIOXIDE LASER CHEMISTRY OF CARBONYL SULFIDE & SELECTED HYDROCARBONS

City University of New York PH.D. 1982

PLEASE NOTE:

In all cases this material has been filmed in the best possible way from the available copy. Problems encountered with this document have been identified here with a check mark __√__.

1. Glossy photographs or pages _____
2. Colored illustrations, paper or print _____
3. Photographs with dark background __√__
4. Illustrations are poor copy _____
5. Pages with black marks, not original copy _____
6. Print shows through as there is text on both sides of page _____
7. Indistinct, broken or small print on several pages _____
8. Print exceeds margin requirements _____
9. Tightly bound copy with print lost in spine _____
10. Computer printout pages with indistinct print _____
11. Page(s) _____ lacking when material received, and not available from school or author.
12. Page(s) _____ seem to be missing in numbering only as text follows.
13. Two pages numbered _____. Text follows.
14. Curling and wrinkled pages _____
15. Other _____

CO_2 Laser Chemistry of Carbonyl Sulfide & Selected Hydrocarbons

by

Alan H. Schwebel

A dissertation submitted to the Graduate Faculty in Chemistry in partial fulfillment of the requirements for the degree of Doctor of Philosophy, The City University of New York.

1982

This manuscript has been read and accepted for the Graduate Faculty in Chemistry in satisfaction of the dissertation requirement for the degree of Doctor of Philosophy.

4/21/82
date

A. M.
Chairman of Examining Committee

29 April 82
date

David C. Locke
Executive Officer

James M. Schulman

Supervisory Committee

The City University of New York

Abstract

CO_2 LASER CHEMISTRY OF CARBONYL SULFIDE AND SELECTED HYDROCARBONS

by

Alan H. Schwebel

Advisor: Professor A. M. Ronn

CO_2 laser excitation of carbonyl sulfide (OCS), both on and off resonance was studied. Fluorescence risetimes and falltimes of the ν_3 mode was monitored after the $2\nu_2$ mode is excited with both an unfocused and focused TEA laser. Activation of this mode is found to be 53 $msec^{-1}torr^{-1}$ under unfocused condition and 23.4 $msec^{-1}torr^{-1}$ under focused excitation. The decay rate constant is approximately 8 $msec^{-1}torr^{-1}$ in both cases. Mechanisms and comparison to results obtained by other methods are discussed in terms of energy gaps and breathing sphere parameters for the processes involved. Under high level excitation (intensity > 10^9 W/cm^2), no dissociation of OCS was detected under collisionless conditions. These results will be discussed in terms of the existing theoretical model of multiple photon dissociation. Laser Induced Dielectric Breakdown of carbonyl sulfide was also studied along with the plasma emission accompanying this process. The spectrum identified the species CO, C_2, and S as the major emitters.

The Laser Induced Dielectric Breakdown Spectrum (LIDBS) of a series of hydrocarbons, fluoromethanes, and chloromethanes was studied using an Optical Multichannel Analyzer (OMA). These spectra were rich in atomic, ionic, and molecular fragments. Each of the spectra were completely identified by matching the emitting line to the literature value of that species. This technique was also used to identify impurities in a mixture of gases.

The CO_2 laser ignition of combustible hydrocarbon mixtures with air or oxygen was studied. The results indicate that laser ignition is successful over a wide range of hydrocarbon percent, and yields less pollutant products as compared to spark ignition. The spectroscopic identification of the visible and near-infrared emission of the flames was also studied. The results are consistent with an electron-type mechanism as the initiator of combustion process.

Dedication

To my parents.

To my mother-in-law.

To the blessed memory of my father-in-law.

To Avrohom, Yisroel, and Esther.

And, most of all --

To my wife, Leah, whose love, devotion, encouragement and, especially, patience made this possible.

Acknowledgements

It gives me great pleasure to express my thanks to Professor Vic Ronn for his scientific guidance and, moreover, for his highly valued friendship. His caring and understanding of matters relating both to science and other things will forever be appreciated.

To the members of Vic's group, both past and present, Barbara, Lenny, Myron, Ross, Shiann, Shu, and Yedidyah, I am thankful for many valuable discussions as well as their continuing friendship. In particular, I must single out one member of the group, Jaime, whose scientific help and close friendship are most treasured. Special thanks go to visiting Professor Jose Riveros for his advice and inspiration during his stay at our laboratory. I am also grateful to Herbie whose help in obtaining the unobtainable will always be remembered.

I would like to also convey my thanks to the professional, administrative, and technical staff of the Chemistry Department at Brooklyn College, especially to Terry for typing this manuscript.

Finally, I must express my sincere gratitude to all the members of my family for their love and encouragement even in the darkest of times.

Table of Contents

Table of Contents

List of Tables

List of Tables (continued)

List of Figures

List of Figures (continued)

CHAPTER 1

Laser Reactions of OCS

Introduction

The role of the laser in chemistry has changed dramatically in recent years. In the early years, after its discovery, laser excited vibrational fluorescence experiments[1] contributed greatly to our understanding of energy transfer processes in single molecules. These experiments utilized readily available low-powered lasers to give information on the rates of excitation and deactivation among the many different vibrational modes of these molecules. The vibrational energy transfer maps generated by this data contributed to the understanding of molecular interactions, helped guide explorations of laser enhanced chemical reactivity, and were also used to improve operation of gas lasers. In the late 1960's and 1970's, the advent of high-powered lasers helped open a whole new field of laser chemistry[2]. These lasers helped to dissociate unique molecular species by relying on the laser's large photon flux, large energy or fluence available, and short pulse duration. Indeed, the stunning laser isotope separation[3] experiments on SF_6 in the early 1970's spawned the belief that an era of mode-selective chemistry had arrived. Chemists envisioned molecules being dissociated by appropriate lasers to give rise to chemical reactions that were not thermally accessible. However, much of this excitement was tempered by the fact that, in almost all cases, the dissociation in such experiments followed the expected fragmentation pattern[4]. In all cases, the weakest bond would rupture regardless of where the energy was deposited. This fact was readily explained by the simple statistical thermodynamical theory referred to as RRKM theory[5]. This theory predicts that, when a molecule absorbs a large number of photons and is elevated to an excited state that is sufficiently high to

dissociate the molecule, fragmentation will occur subsequent to vibrational equilibration of all vibrational degrees of freedom. This means that, after the laser energy is deposited in a specific vibrational state and then the molecule is elevated to a more highly excited stated before dissociation, there is total excitation of all vibrational degrees of freedom and not only the one that was initially excited. Such a condition would lead to fragmentation along a dissociation coordinate that is weaker than the rest. To illustrate this point, if one was to perform an experiment on a molecule such as SF_5Cl, we would expect the sulfur-chlorine bond to fragment since it is the weakest in the system. Indeed, this prediction is borne out by an experiment in which the sulfur-fluorine vibration was excited but the sulfur-chlorine bond was ruptured[6]. In general, it is now believed that multiple photon dissociation (MPD) experiments do not lead to a fragmentation pattern that is in any way different than that predictable or achievable via other techniques.

Chemists then began turning their view to the fundamental studies of both multiple photon excitation and dissociation of polyatomic molecules with a single infrared laser frequency[7]. Many studies, both theoretical and experimental, were done allowing us to determine the molecular and laser properties that most strongly influence the multiple-photon process.

At the same time these multiple-photon experiments were being done, chemists took note of another laser process called laser-induced dielectric breakdown[8] (LIDB). LIDB is a phenomenon found when an infrared laser of high power density is focused into a polyatomic gaseous sample. A simple explanation of this process is that electrons

accelerated by the large AC electric field of the laser achieve sufficient energy to cause both fragmentation and isomerization of polyatomic species. Most often, basic experimentalists in the MPD discipline avoided dielectric breakdown, believing that the formation of large concentrations of ions and electrons would affect the mechanism of dissociation. However, recent work has shown that LIDB experiments do not result in any different fragmentation pattern than MPD[8]. If one is to compare techniques with the same molecule, one could visualize an experiment on SF_5Cl in which a laser beam is focused into a pressurized cell at high enough pressure to insure dielectric breakdown and follow the fragmentation pattern. Indeed, it is found that the sulfur-chlorine bond (the weakest one) once again ruptures as in the multiple-photon experiment. Obviously, despite the similarity of the final fragmentation process, there are many fundamental differences in LIDB and MPD. For instance, in the MPD case, excitation proceeds via resonant absorption of the laser photon while, in LIDB, no such resonant interaction is necessary. It is, in fact, preferable that the molecule under investigation has no resonant level near the laser wavelength since the electric field that accelerates the electrons would be somewhat depleted by an absorption, should one exist. Other differences such as low gas pressure (MPD) versus high gas pressure (LIDB), low power (MPD) versus high power (LIDB) also exist.

Given the similarities and differences between LIDB and MPD, we felt it would be important to do a systematic study of these two processes on one molecule so as to measure the lifetime of any ions, electrons, and fragments that may occur in each of these processes.

The simplest molecule possible to be used in trying to give a detailed description specifying the state involved in the dissociation mechanism was carbonyl sulfide (OCS).

OCS is a linear triatomic molecule about which much is known. Its infrared spectrum was studied completely enough to allow a determination of all of the anharmonicity constants of this molecule[9]. The overtone of its bending vibration matches the P(22) 9.6 line of the CO_2 laser[10].

This triatom should dissociate simply into carbon monoxide and sulfur both by multiple-photon dissociation and dielectric breakdown. By following the lifetimes of the CO and S fragments found in both cases, we hoped to be able to make quantitative comparisons between MPD and LIDB.

In order to have a complete picture of the interaction of laser radiation with OCS, we first did some energy-transfer studies under low-excitation conditions before performing the dissociation experiments both "on" and "off" resonance. In the next section, I will give a more detailed theoretical background of the energy transfer, multiple photon dissociation, and laser induced dielectric breakdown processes, followed by the results and discussion of the experiments.

Theoretical Background

A. Energy Transfer

The flow of energy between the various degrees of freedom of a molecule is a topic of crucial importance in the development of a complete theory of chemical reactivity. In fact, the relative rates of energy flow between vibrational modes and among the translational, rotational, and vibrational degrees of freedom help determine the gain, energy, and power characteristics of most infrared gas lasers. In this section, we will review some of the theoretical aspects of energy transfer with particular emphasis on the factors governing the intermode vibrational energy transfer in polyatomic molecules.

The transfer of energy between vibration and translation is a collisional process since it is only at molecular collisions that energy can be exchanged. The transition probability (P) is the probability that, at a collision, a given process will take place, i.e., a vibrational quantum will be converted entirely to translational energy or else converted into a quantum of a different vibration. The theory which has been most widely used for quantitative comparison with experimental measurements of vibrational relaxation is the Schwartz, Slawsky, and Herzfeld (SSH) theory. The theory was first developed for diatomic molecules[11] and then extended for polyatomic molecules by Tanczos[12] in 1956.

The probability that, during a binary collision, vibrational mode (a) of one molecule will change its quantum state from i to j, while simultaneously a second mode (b) in another molecule will change its state from k to ℓ is given by SSH theory as:

$$P^{i-j(a)}_{k-\ell(b)} = P_o(a)P_o(b)[V^{ij}(a)]^2[V^{k\ell}(b)]^2(4\mu/kT)$$

$$x \quad \exp[-\varepsilon/kT]\left(\frac{8\pi^3\mu\Delta E}{h^2}\right)^2 \int_0^\infty f(\bar{u})d\bar{u} \qquad (1)$$

where $$f(\bar{u}) = \frac{\bar{u}}{\alpha^4}\left(\frac{r_c}{\sigma}\right)^2 \exp\left[-\frac{\mu\bar{u}^2}{2kT}\right]\left\{\frac{\exp[L-L']}{1-\exp[L-L']^2}\right\},$$

$$L = \frac{4\pi^2\mu}{\alpha h}\cdot\bar{u} \quad \text{and} \quad L' = \frac{4\pi^2\mu}{\alpha h}\cdot\bar{V},$$

μ is the reduced mass of the colliding pair which approach one another with an effective relative velocity, $\bar{u}$, and recede with velocity, $\bar{V}$. The integration is over the thermal distribution at T of the molecular velocities. ΔE is the amount of energy exhanged between the vibrational and translational degrees of freedom in the V-T case, i.e.,

$$\Delta E = h\nu_a(i-j) \qquad (2)$$

since $k = \ell$. In the case of vibration-vibration transfer (v-v),

$$\Delta E = h\nu_a(i-j) + h\nu_b(k-\ell) \qquad (3)$$

When ΔE is large, the integration can be solved analytically in terms of α^* to give the formula deduced by Tanczos which is valid for values, $\Delta E > 200$ cm^{-1}. This equation is

$$P_{k-\ell(b)}^{i-j(a)} = P_o(a)P_o(b)\left(\frac{r_c^*}{\sigma}\right)^2 [V_{(a)}^{ij}]^2 [V_{(b)}^{k\ell}]^2 8\left(\frac{\pi}{3}\right)^{\frac{1}{2}}$$

$$\left[\frac{8\pi^3 \mu \Delta E}{\alpha^{*2} h^2}\right] \xi^{\frac{1}{2}} \exp\left[-3\xi + \frac{\Delta E}{2kT} + \frac{\varepsilon}{kT}\right] \qquad (4)$$

where $$\xi = \frac{\mu u^{*2}}{2kT} = \left(\frac{\Delta E^2 \mu \pi^2}{2\alpha^* h^2 kT}\right)^{\frac{1}{3}}$$

This equation can be considered in four parts: (a) the geometrical or steric, factor P_o (b) the collision cross-reference factor (r_c^*/σ^2) (c) the vibrational factors $[V]^2$ (d) the translational factor represented by the remainder of the equation.

(a) The steric factor, P_o, is required to account for the fact that the molecules are not spherically symmetrical and that some collisional orientations will be more effective than others. They are usually taken as 1/3 (the average of $\cos^2 \theta$ taken over a sphere) for diatomics and for longitudinal vibrations of linear polyatoms. For non-linear polyatoms and for bending modes of linear molecules, P_o is taken as 2/3.

(b) The collision cross reference factor, (r_c^*/σ^2), is the ratio of the intermolecular separation at the classical turning point to the separation at zero potential energy, σ, which is used in calculating the gas kinetic collision number, Z, where

$$Z = 4n(\sigma^*)^2 \pi kT(m)^{\frac{1}{2}} \qquad (5)$$

(c) The vibrational factor $[v^{ij}(a)]^2$ is the square of the matrix element for the transition between the two vibrational states, i, j, of molecule (a). It represents the coupling of the initial and final states, i and j, of the oscillator under the influence of the perturbation produced by the collision. It depends on the repulsion parameter, α, and the frequency and amplitude of the vibration. Vibrational factors are defined for zero, single, and double quantum jumps as

$$[v^{i-i}]^2 = 1 \tag{6}$$

$$[v^{(i+1)-i}]^2 = [v^{i-(i+1)}]^2 = \alpha^2(\bar{A}^2)(i+1)/2\gamma \tag{7}$$

$$[v^{(i+2)-i}]^2 = [v^{i-(i+2)}]^2 = \alpha^4(\bar{A}^4)(i+1)(i+2)/16\gamma^2 \tag{8}$$

where $\gamma = 4\pi^2\nu/h$.

The vibrational amplitude coefficient (A^2) is the Cartesian displacement of an atom for unit change of the normal coordinate of a given vibration. The values of (A^2) for the surface atoms of a molecule, which is treated as a "breathing sphere," are then averaged and summed over the number of surface atoms to give $(\bar{A}^2)$. The magnitude of the whole matrix element $[V^{(i+1)-i}]^2$ corresponding to a one quantum jump varies directly with α^2 and $(\bar{A}^2)$ and inversely with the vibration frequency.

(d) The translation factor gives expression to the change in kinetic energy of translation involved in the inelastic collision. The

parameters involved are the reduced mass of the collision, μ, and the temperature, T, which together determine the velocity of approach; ΔE, the amount of vibrational energy transferred in the collision, and the intermolecular repulsion parameter, α.

For v-v transfer between different molecular species, the additional probability arises of a resonant transition when

$$h\nu_a(i-j) = h\nu_b(k-\ell),$$

and $\Delta E = 0$. For resonant and near-resonant transfer, a different analytical solution also due to Tanczos, applies for values of $\Delta E \lesssim 50\ cm^{-1}$.

$$P^{i-j(a)}_{k-\ell(b)} = P_o(a)P_o(b)[V^{i-j}(a) \cdot V^{k-\ell}(b)]^2 \frac{64\pi^2\mu kT}{\alpha^2 h^2}\exp[\epsilon/kT] \qquad (9)$$

Resonant transfers are much faster than non-resonant transfers and there is no term in ΔE so that all near resonant transfers with $\Delta E \lesssim 50\ cm^{-1}$ behave as though resonant. Dependence on the frequency of the exchanging modes arises through a pre-exponential term, $[V^{i-j}(a)\cdot V^{k-\ell}(b)]^2$. Since each squared vibration factor for a single quantum transition, $[V^{(i-\ell)-i}]^2$, is inversely proportional to frequency (equation 7), this gives rise to inverse dependence of P on the square of the frequency. Resonant transfers between high frequency modes will thus have a collision probability much smaller than unity.

We stated earlier that intramolecular transfer of energy between different vibrational modes can occur only in collision as the energy discrepancy between the modes must be made up as translational energy.

For a molecule with two active vibrational modes of frequency, ν_1 and ν_2, there are three possible vibrational transitions which are illustrated on the energy-level diagram in Figure 1.

(a) Transfer of translational energy into $0 \rightarrow 1$ excitation of the mode ν_1 with relaxation time β_1.

$$A^*\nu_1(v=1) + A \underset{\rightarrow}{\leftarrow} A(v=0) + A + \Delta E_1 \qquad (10)$$

(b) Transfer of translational energy to $0 \rightarrow 1$, excitation of the mode ν_2 with relaxation time β_2.

$$A^*\nu_2(v=1) + A \underset{\rightarrow}{\leftarrow} A(v=0) + A + \Delta E_2 \qquad (11)$$

(c) The complex transfer of one quantum of vibrational energy from mode ν_1 plus the necessary increment of translational energy to give $0 \rightarrow 1$ excitation of the mode ν_2 with relaxation time β_{12}.

$$A^*\nu_1(v=1) + A \underset{\rightarrow}{\leftarrow} A^*\nu_2(v=1) + A + \Delta E_{12} \qquad (12)$$

The values, β_1, β_2, and β_{12} in principle can be calculated using SSH theory. Since only one molecular species is involved in all three processes, their relative magnitudes will be mainly determined by the value of ΔE. For the case of Figure 1, the fastest relaxation process will be the complex transfer (c) and the slowest the V-T relaxation of the ν_2 by process (b). This means that $\beta_2 > \beta_1 > \beta_{12}$. Thus, vibrational energy enters the molecule via process (a) which is

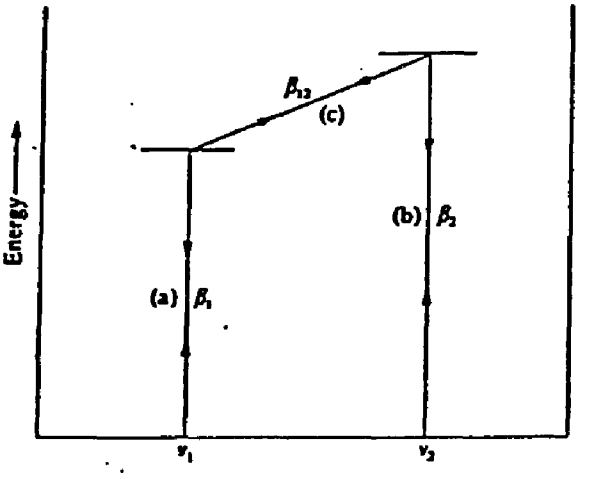

FIGURE 1

Energy Level Diagram Showing Transitions for a Molecule With Two Active Vibrational Modes

rate controlling and rapidly flows in complex collisions via the faster process (c) to the upper mode. Process (b) is too slow to play any role. This is known as a series mechanism and is characterized by a single overall relaxation time, β, which can be related to β_1 by

$$\beta_1 = (C_1/C_s)\beta \tag{13}$$

where C_1 is the heat capacity contribution due to mode ν_1 alone and C_s the total vibrational heat capacity.

This kind of behavior is shown by the majority of small polyatomic molecules. The most usual pattern of fundamental vibration frequencies is such that the energy gaps between the upper modes are much less than the energy level of the lowest mode. The general picture is that rapid v-v transfer maintains continuous equilibrium of vibrational energy between the various fundamental modes of the molecule and that the whole of this energy relaxes in a single vibration-translation transfer process via the lowest mode. In practice, infrared laser induced fluorescence experiments offers a unique opportunity to study the rate of energy transfer between various modes of a polyatomic molecule. After pumping a certain resonant transition of the molecule, the rate of increase of fluorescence for a given level following excitation is a measure of the v-v energy transfer rate between modes, while the decay of fluorescence is related to the V-T energy transfer rate.

B. Multiphoton Absorption and Dissociation

It is now well known that a molecule can sequentially absorb enough infrared photons to successfully drive a chemical reaction. It has been shown experimentally that, under collisionless conditions[13], a

molecule may absorb thirty or more photons, dissociate, and even maintain its isotopic selectivity[14]. Many theoretical explanations have been advanced in recent years to interpret these experimental findings[15]. The understanding of these processes requires the explanation of the following points:

(a) Anharmonicity Effects

Since only a single vibrational mode of the molecule is in resonance with the laser frequency, the question arises how does one overcome the inherent anharmonicity of this mode with the monochromatic laser light.

(b) Intrastate Scrambling Effects

The description of the level structure of the lowest potential surface of a polyatomic molecule in terms of independent anharmonic oscillations is expected to break down at some energy above the electronic origin because of intrastate coupling between different modes. The question is what effect does this vibrational scrambling have on the multiphoton process.

(c) Field Effects

Multiphoton molecular photodissociation was observed in intense electromagnetic fields. Therefore, we must also address the effect of these fields on the process. The important field effects are:

(1) Stark Effect[16]. In the large electric field present in the TEA laser, absorption line broadening due to a splitting of molecular vibrational-rotational sublevels occurs. This broadening is a result of the dynamic Stark Shift which can compensate for anharmonicity effects of the low-lying levels. The magnitude of this

splitting for a diatomic molecule is given by[17]

$$\Delta\tilde{\nu} = (B_e/2)(\mu E/h\nu)^2, \text{ cm}^{-1} \quad (14)$$

where B_e is the rotational constant in cm^{-1}, μ is the transition dipole moment in Debye, E is the electric field strength, and ν is the laser frequency. This effect can be quite large for molecules with large dipole moments and large rotational constants.

(2) Power Broadening. The multi-level power broadening arises because a transition between oscillator levels occurs in a time which is short compared to the time in which the laser field gets out of phase with the oscillator. This effect is determined by the Rabi frequency[17], and the detuning of $\nu - \nu_o$ where ν is the laser frequency and ν_o is the oscillator frequency. The Rabi frequency is defined as

$$\nu_R = \mu E_o/h \quad (15)$$

where E_o is the time independent field strength, μ is the transition dipole moment, and h is Planck's constant. Excitation of an oscillator is proportional to the square of the term, $\nu_R/(\nu-\nu_o)$. Therefore, if the anharmonicity of the pumped modes is small compared to the Rabi frequency, then high vibrational levels can be populated in short times.

We can now proceed with our discussion of the problem of multi-photon photofragmentation of an isolated molecule on the lowest electronic potential surface. In a polyatomic molecule, we can

distinguish three energy regions in the order of increasing energy. Region I is the low energy range where there is a sparse level distribution. In this region, the density of background states is low so intrastate scrambling of the pumped vibrational states with other states is trivially small. In this coherent region, power broadening effects will be of the most importance. In region II, there is a mixing of states between the pumped state and the dense background states. This region is known as the quasicontinuum[18] and can be pumped by incoherent excitation. The onset of the quasicontinuum will depend on the density of states at that energy level. In this region, the rates of intramolecular vibrational relaxation and redistribution relative to the rate of the photofragmentation process are important. Region III is the true continuum of levels above the dissociation limit.

Two models have been proposed to explain the excitation in the coherent region (Region I). The first model[19] is based on a combination of the effect, triple-vibrational-rotational resonance or PQR transitions with the effect of non-resonance absorption at the transitions in the vibrational quasicontinuum of a polyatomic molecule. The first three induced transitions of a molecule can be in exact resonance with the field, the frequency of which is tuned to the Q branch, the transition $v = 1 \rightarrow v = 2$. Despite vibrational anharmonicity, this is achieved by compensation for the anharmonic shift of the transition energy by a shift in the opposite direction which results from a change in the rotational state. After the molecule is excited to $v = 3$, the density of the levels becomes high enough so as to form a quasicontinuum region. In this region,

excited molecules can directly absorb enough photons, if the power is high, without requiring a resonant field to reach the continuum dissociation limit. Since, in the case of triple resonance, high intensities are not required to excite the level, v = 3, the dissociation threshold intensity depends on the molecular excitation in the quasicontinuum which demands high densities of laser pulse energy.

The second model[20] assumes that the molecule can be excited from the vibrational ground state via the anharmonic ladder where field effects compensate for anharmonicity. Since anharmonicity is mostly overcome by the Rabi frequency, the power intensity is more important than power density in this region. At v = 3-4, the vibrational density of states is considered to be sufficiently large and the vibrational energy will spread out into a quasicontinuum of hot bands. The spread of energy among the vibrational modes in Region II involves a complete intrastate vibrational internal energy redistribution, which can be specified by an effective vibrational temperature, T*. T* is subsequently increased by a sequence of one-photon absorption processes until the photodissociation threshold is reached. The RRKM theory of unimolecular reaction[5] is then applied and the familiar Arrehenius equation provides the quantitative rate calculation for this unimolecular dissociation. One of the common features of both these models is that, at some intermediate energy range, there must be a sufficient density of energy levels so as to ensure that incoherent excitation can lead to collisionless dissociation of a polyatomic molecule. Therefore, it would seem unlikely that diatomic or possibly even triatomic molecules would be dissociated by infrared laser absorption. We will return to this point later in our discussion.

C. Laser Induced Dielectric Breakdown

Unlike the energy transfer and multiphoton dissociation processes, another interaction of CO_2 laser radiation with molecules is observed even when there is no resonant absorption. This process of laser induced dielectric breakdown (LIDB) can occur when the laser radiation interacts with the gas molecules leading to the onset of electrical conductivity in a normally non-conducting gas. Laser induced gas breakdown is always accompanied by the emission of intense light lasting longer than the laser pulse. The generally accepted model for the mechanism of CO_2 laser induced breakdown is the avalanche breakdown mechanism[21]. This theory presumes the existence of initial electrons which are accelerated via the high electromagnetic field by inverse Bremsstrahlung[22] until they acquire sufficient energy to ionize the gas molecules. The initial electrons can be available due to external sources, i.e., exoelectrons, cosmic light, etc. It is also possible that impurities in the gas sample can be photoionized relatively easily giving rise to these initial electrons.

Since breakdown can occur without matching the laser frequency with the vibrational frequency of the reactant molecule, the gas is effectively transparent to the laser light. However, when a plasma is formed, the motion of the electrons and ions in specific electrostatic oscillation is characterized by the plasma frequency (Langmuir frequency), ν_p. The equation of motion which defines the frequency, ν_p, of the electrostatic oscillation of the electrons leads to the relation[22]

$$\nu_p^2 = 4\pi e^2 n_e / m_e \qquad (16)$$

$$\nu_p(\text{sec}^{-1}) = 5.65 \times 10^4[n_e(\text{cm}^{-3})]^{\frac{1}{2}} \qquad (17)$$

where e, m_e, and n_e are charge, mass, and density of electron respectively. From the macroscopic theory of a plasma, in which the plasma is considered to be composed of two continuous fluids, electrons, and ions. These are described by time dependent function of the density n(r,t), velocity v(r,t), and temperature T(r,t) in the presence of a monochromatic field and induced plasma current, the complex refractive index $\tilde{n}$ is given by[22]

$$\tilde{n}^2 = 1 - \frac{\nu_p^2}{\nu(1+i\nu_e/\nu)} \qquad (18)$$

Here ν is the electromagnetic wave frequency, ν_e is the collision frequency between the fluids, and i is the imaginary unit. For a collisionless plasma ($\nu_e = 0$), the refractive index vanishes as the plasma frequency, ν_p, equals the laser frequency, ν. The plasma is transparent only if $\nu > \nu_p$; otherwise, the incident electromagnetic wave is totally reflected by the plasma. The frequency, $\nu = \nu_p$, is called the critical frequency which via equation (16) defined electron density of the plasma, called the critical density. Thus, at the critical frequency, total energy absorption occurs. For the CO_2 laser frequency, the critical density is 10^{19} electrons/cm^3 according to equation (17). The plasma density behind the ionization front is equal to the neutral density of the original gas. Experimental evidence has shown that this critical pressure is generally several times larger than the threshold pressure necessary to induce breakdown[23].

On the basis of avalanche theory, the power density required for breakdown is given as[24]

$$(P/A) = \frac{2m_e \varepsilon c I_p \nu^2 \ln (n_e/n_o)}{e^2 \nu_e \tau} \qquad (18)$$

where: P = radiation power (Watts)

A = area (meter^2)

m_e = electron mass (9.1×10^{-31} kg)

ε = free space permittivity (8.85×10^{-12} Coul^2/ntm^2)

c = speed of light (3×10^8 m/sec)

I_p = ionization potential of gas (Joules)

ν = radiation frequency of the field (sec^{-1})

n_e = final electron density (m^{-3})

e = electronic charge (1.60×10^{-9} Coul)

ν_e = electron-atom collision frequency (sec^{-1})

τ = duration of laser pulse (sec)

The threshold power is variable with different gases at different pressures. For a gas at constant pressure, the threshold power is affected by external preionization. In general, preionization by the electrical discharge will reduce the threshold laser power[24] because the initial electrons needed for avalanche ionization were provided by the injection of free electrons into the focal volume.

Another interesting point about laser induced plasma is that there exists different threshold pressures for different molecular species. Threshold pressure conditions are linked to the molecular properties of the gas, such as polarizability, dipole moment, and ionization

potential[25].

The most important feature of LIDB is that it allows the laser chemist to dissociate molecules which have no resonant absorption. However, this nonresonant process, which is non-selective in mode excitation, always yields thermodynamically controlled product formation. In fact, in almost all cases, the final products from multiphoton dissociation and from laser-induced dielectric breakdown are the same[25]. It was with this in mind that we undertook the study of both the multiphoton dissociation and laser-induced dielectric breakdown of OCS to compare the energy content of the products of these two processes. In both cases, the products should be CO and S and, by studying the energy content of both the CO and S, we hoped to elucidate a greater understanding of both these processes.

Experimental

A schematic diagram of the experimental apparatus is shown in Figure 2. Two different TEA CO_2-N_2-He lasers were used in the experiments. For the energy transfer and dielectric breakdown experiments, a home-built Rogowski-type TEA laser, oscillating over many of the rotational-vibrational lines of the P and R branches of both the 9.6 μ and 10.6 μ CO_2 laser bands was employed. For the energy transfer experiments, the laser was tuned to the P(22) 9.6 transition to coincide with the $2\nu_2$ vibration of OCS. This laser line had an average energy output of 0.3 to 2.0 Joules per second. A typical oscilloscope trace of one such pulse as measured by a HgCdTe (77 K) detector is presented in Figure 3. A copper mirror of 10 m focal length was used to collimate the beam within the glass cell used in the experiments. A glass cell of 45 cm^3 fitted with NaCl windows at either end and having a KBr window in the center was used to monitor the infrared fluorescence. The gases were Matheson research grade with stated purities as OCS (97.5%), CO (99.5%), and Ar (99.995%). Further purity was achieved by repeated vacuum distillation of the sample prior to each measurement.

Fluorescence was detected at right angles to the beam axis and was monitored as a function of time after excitation. An InSb (Spectronics) photovoltaic detector cooled to 77 K and terminated with a 50 Ohm load was used to observe the emission in the 5 μ region. For very weak signals, an Advanced Kinetics amplifier was used before the signal was displayed on an oscilloscope (Tektronix Model 7704A) and then photographed for analysis. The response time for the detector and associated electronics was less than 1 μsec.

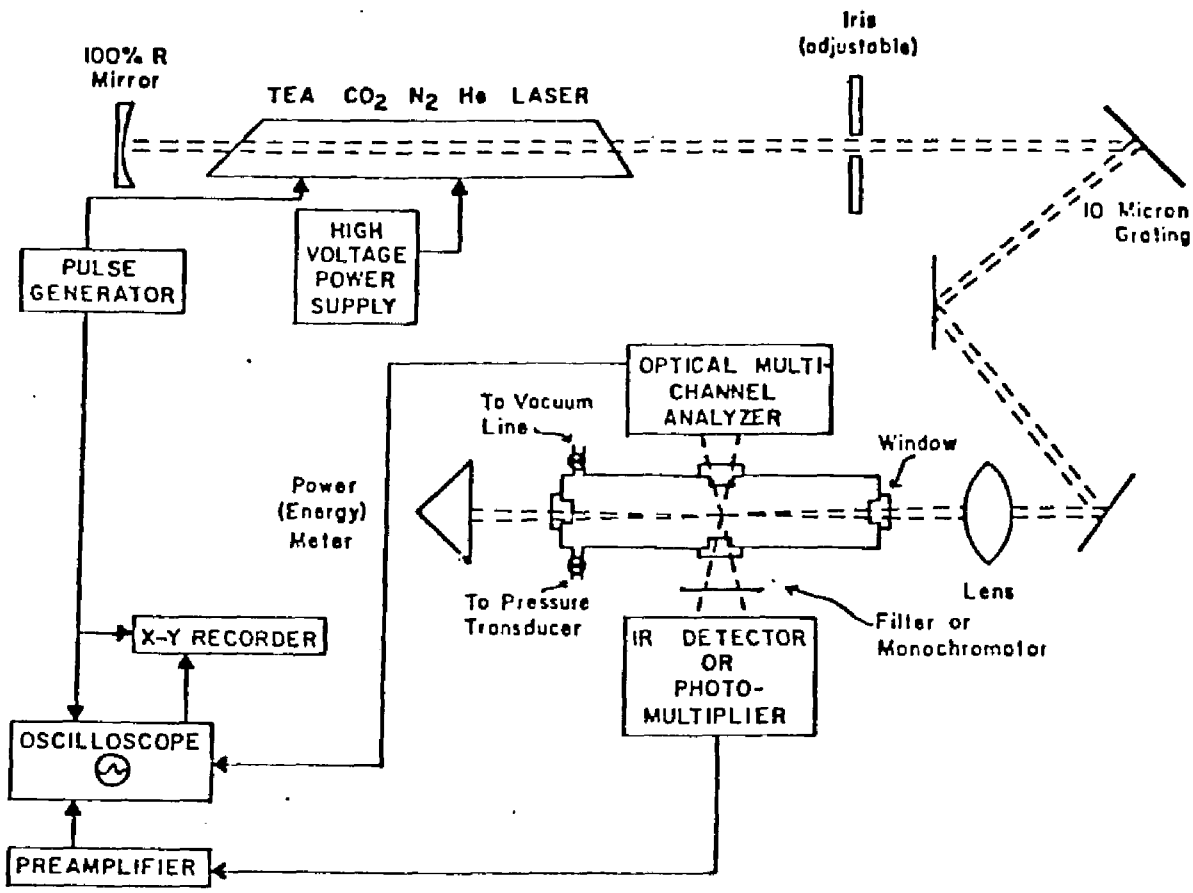

FIGURE 2

Experimental Set-up

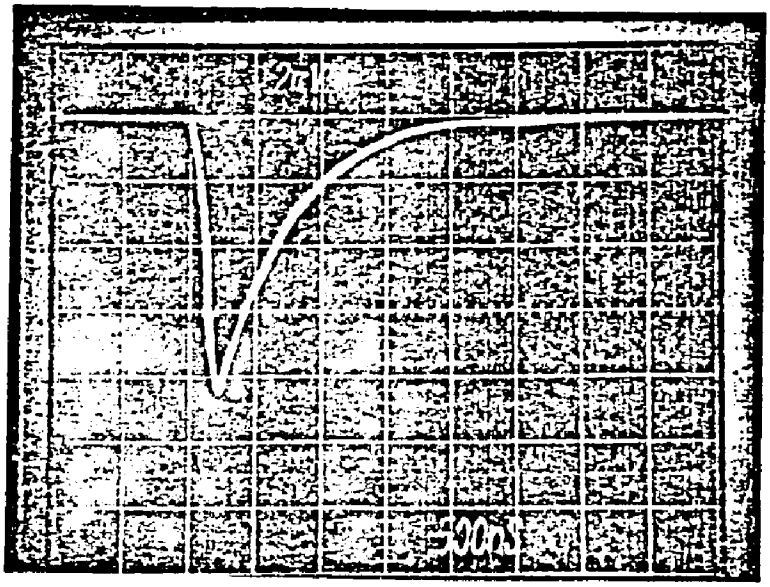

FIGURE 3

CO_2 TEA LASER PULSE - R(20) 10.6μ - 2.0 W (AVERAGE POWER)

At a given pressure, the rate of rise or fall of the fluorescence signal was obtained as $1/\tau$ from a plot of emission intensity versus time displayed on the oscilloscope. From an examination of the formula of an exponential curve.

$$y = Ae^{-kt} \tag{19}$$

where y is the amplitude at any time, t, A the maximum amplitude, and $k = 1/\tau$, the decay rate constant, it's apparent that τ is the relaxation time, defined as the time ($t = \tau$) required for the signal to decay to 1/e of its initial value. The uncertainty of the calculated rates are ±25%.

For the multiphoton absorption and multiphoton dissociation experiments, a Lumonics TEA laser (model 203) was used. With a pulse length of 300 nanoseconds FWHM and 700 nanoseconds tail, output of up to 15 Joules was possible. When N_2 was removed from the gas mixture, laser energies of 3 J in less than 100 ns were obtained. The beam was then focused into the reaction cell using either a 5 in. focal length ZnSe lens or a 10-inch focal length Ge lens. By measuring the burn pattern of the focused laser, it was determined that the focal point was less than 0.01 cm^2 in area. At the focal point then, the intensity of the laser is in the gigaWatt/cm^2 range.

Since particulates of S are expected to be the final product, the formation of these particulates were investigated by light-scattering techniques. A He-Ne laser was directed through the reaction cell both colinear and at right angles to the CO_2 laser beam. If particles were formed, reflected points should be observed due to the scattering of the He-Ne beam by the particles. These points were looked for both

by eye and by use of a photomultiplier tube with a 6328 Å laser filter. Further product analysis was carried out using an infrared spectrophotometer (Beckman IR-10) and a mass spectrometer (Varian CH-7). In all experiments, gas pressure was monitored using a capacitance manometer mounted on the cell.

Visible spectrum of the breakdown process were recorded using an RCA photomultiplier (model 341034) coupled to a grating monochromator (Spex Model 1215) with a resolution of 10 nm. Emission at wavelengths shorter than 3500 Å was observed using an EMI phototube (model 9683QB). All signals were displayed on an oscilloscope (Textronix Model 7704) and were signal averaged for a minimum of 10 shots.

Results

A. Energy Transfer

Figure 4 shows a partial vibrational energy level diagram for OCS. The pumped level is $2\nu_2$ which is the overtone of the bending mode. Fluorescence in the 4.65 - 5.15 μ region was studied using an InSb detector and a narrow bandpass filter. This region contains both fluorescence at 4.94 μ from the ν_3 asymmetric stretch and at 4.812 μ from the $4\nu_2$ level. However, those two signals could not be resolved and the stronger ν_3 fluorescence undoubtedly comprises most of the signal. The fluorscence was significantly absorbed ($\sim$ 70%) by OCS placed in a filter cell between the fluorescence cell and the InSb detector. This result implies that, even under TEA laser excitation, the fluorescence derives primarily from a transition to the ground state. A plot of both the activation and deactivation of ν_3 versus OCS pressure is given in Figures 5 and 6. The rate constant for the activation, which is the slope of the line calculated by the least-square method is 54 ± 10 msec^{-1}torr^{-1}. For the deactivation, the rate constant is 9 ± 2 msec^{-1}torr^{-1}.

The results given above are for unfocused TEA laser pumping. A study of transfer rates was also done under focusing conditions by using a 10-inch focal length Ge lens. In this case, we could expect to populate even higher vibrational levels and the exact origin of the fluorescence is not perfectly clear. The results of the focused laser pumping are given in Figures 7 and 8 for both the rise and fall as a function of OCS pressure. The values of all the rate constants measured for OCS is shown in Table 1.

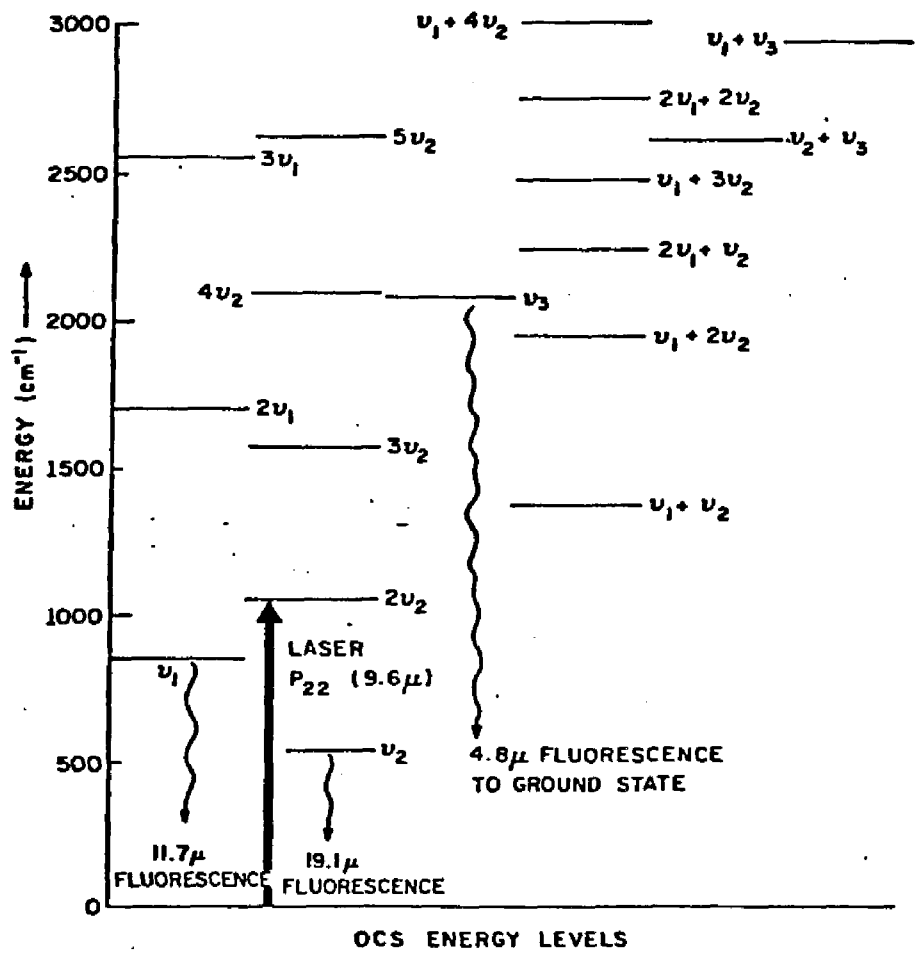

FIGURE 4

Partial Diagram of OCS Energy Levels

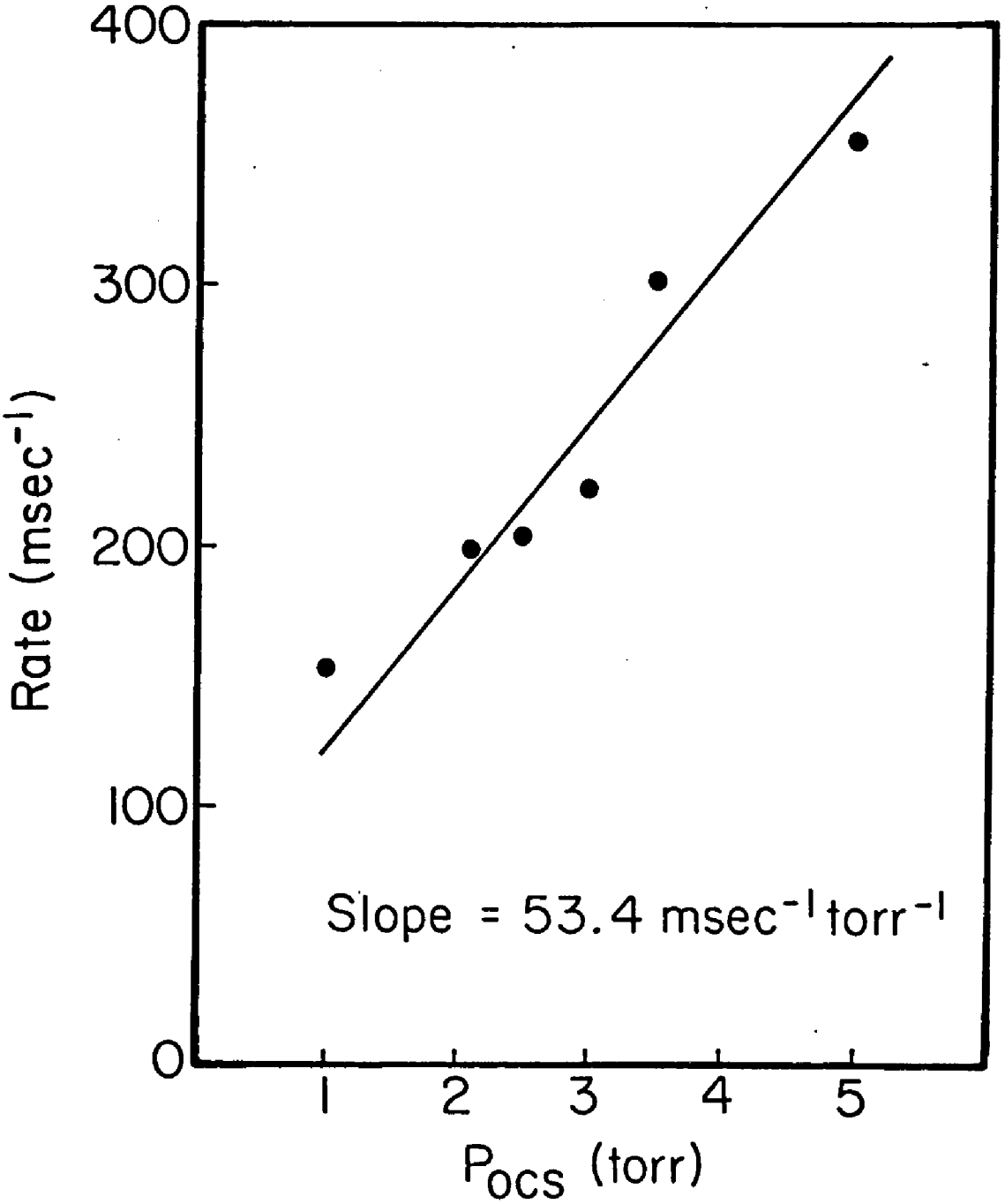

FIGURE 5

OCS ν_3 Activation - Unfocused

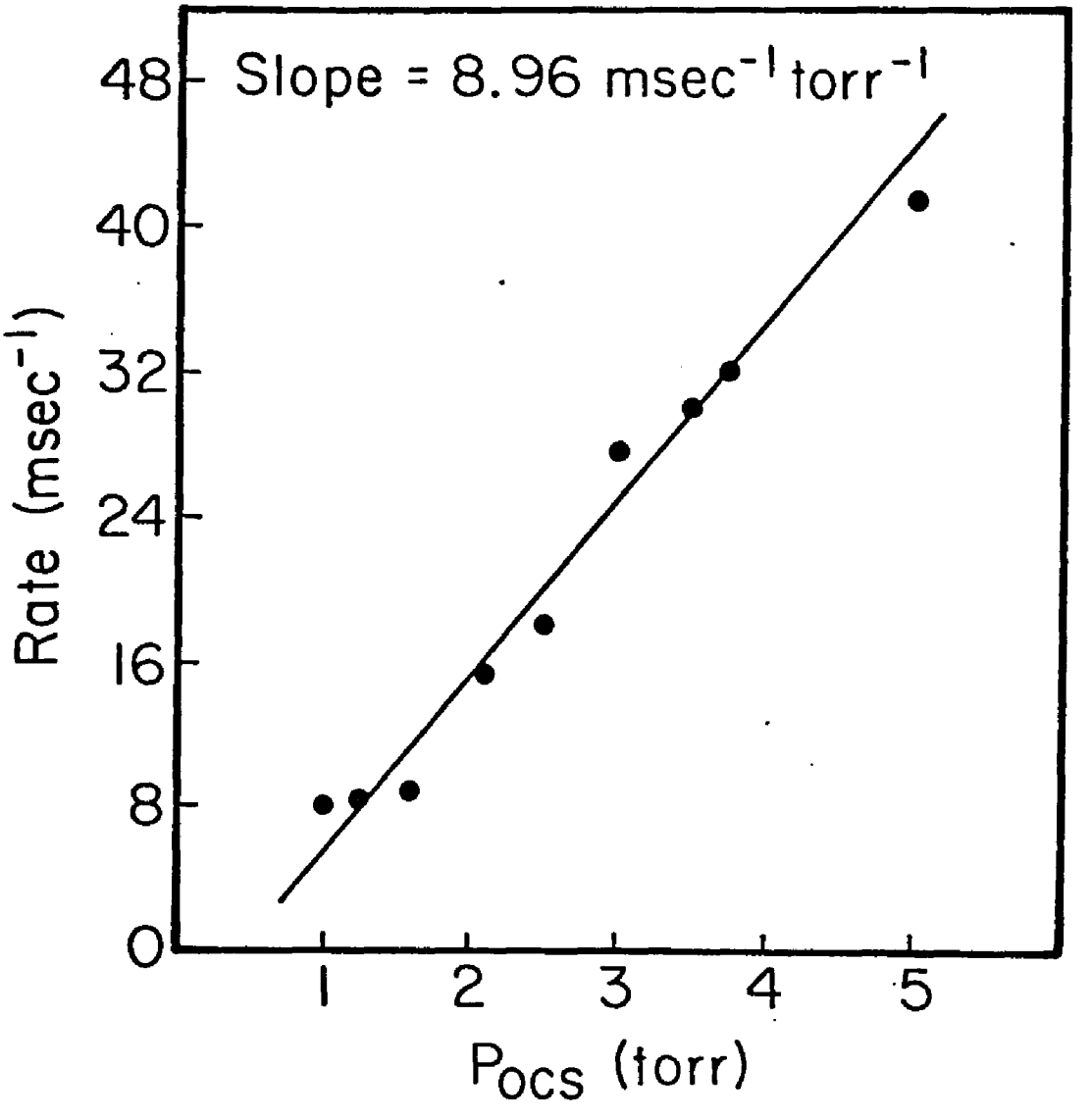

FIGURE 6

OCS ν_3 Deactivation - Unfocused

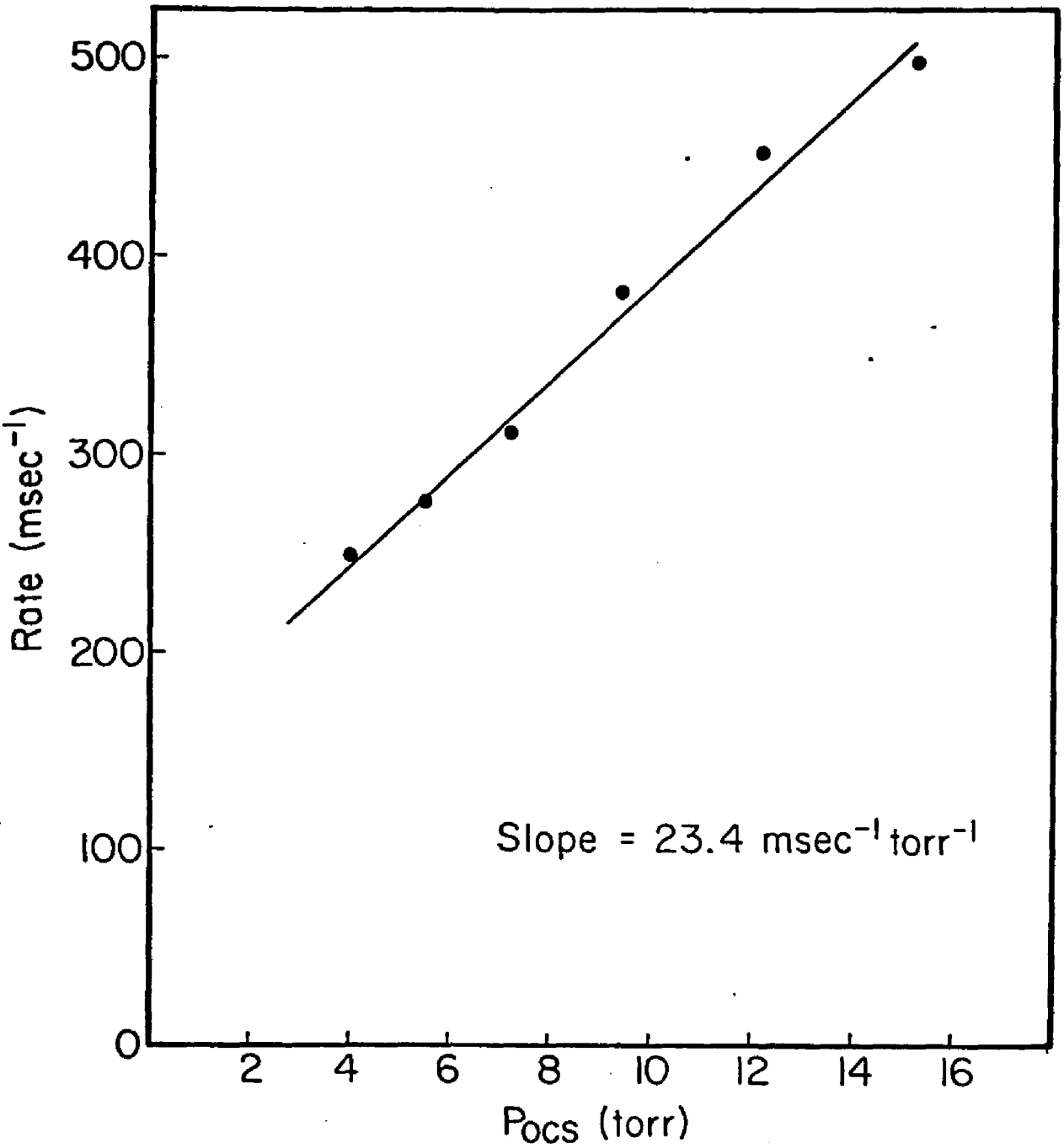

FIGURE 7

OCS ν_3 Activation - Focused

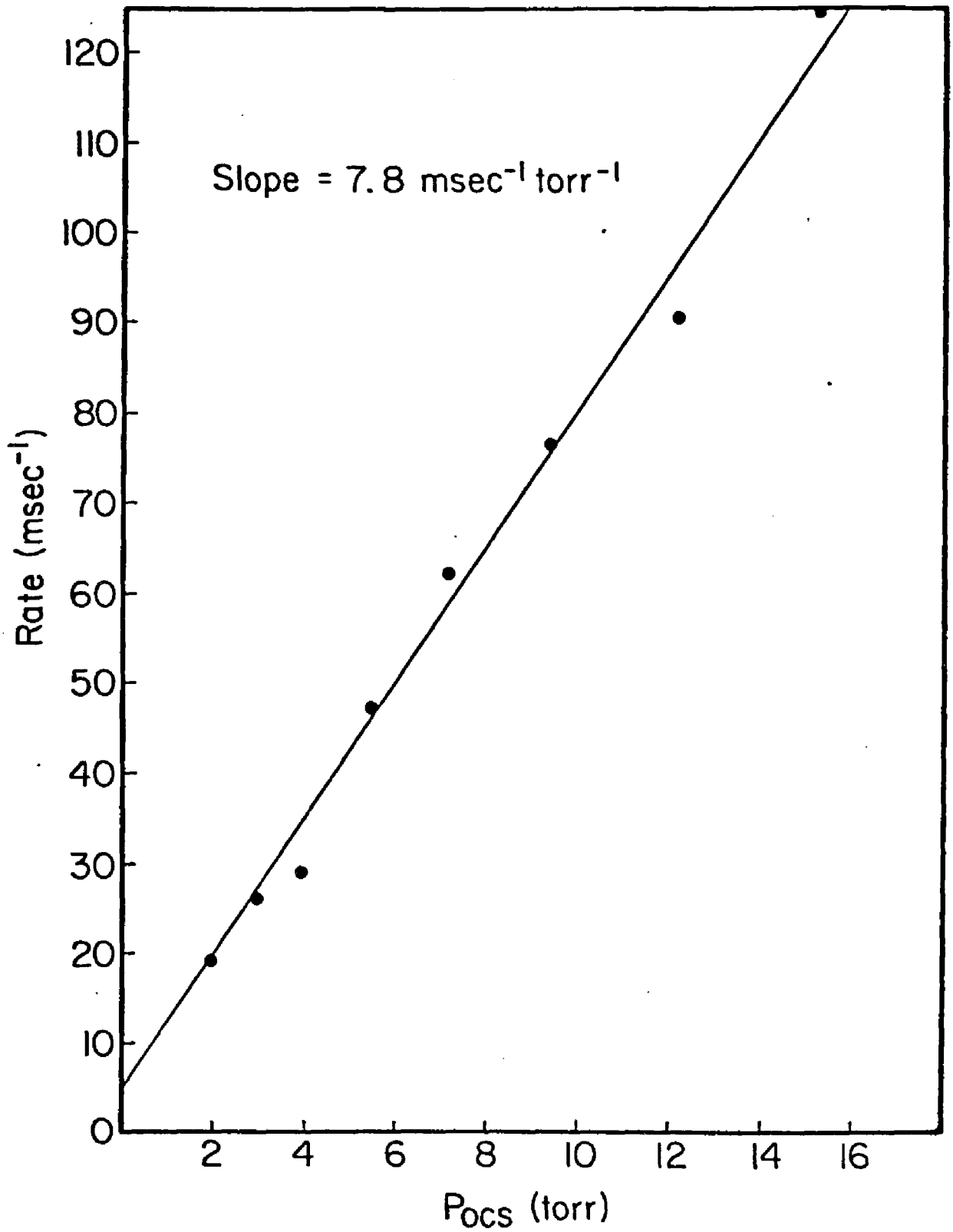

FIGURE 8

OCS ν_3 Deactivation - Focused

Table 1

Measured OCS Rate Constants

Process	Collision Partner	Rate Constants ($msec^{-1} \cdot torr^{-1}$)
ν_3 unfocused		
activation	OCS	54 ±10
deactivation	OCS	9 ±2
ν_3 focused		
activation	OCS	23.4 ±3
deactivation	OCS	7.8 ±2

Infrared fluorescence was also observed using unfocused excitation at higher pressures of OCS (5 - 20 torr). It was found that a second signal appeared approximately 100 μsec after the ν_3 fluorescence and had a risetime of ∿ 80 μsec at 13 torr and a very long decay time (> 1 ms) at that pressure. The delay time between the ν_3 fluorescence and the second signal was decreased with increasing fluence and also, upon addition of Ar. This fluorescence originates from either the $\nu_1 + 2\nu_2$ or $2\nu_1 + \nu_2$ combination bands of OCS (Figure 4).

B. Multiphoton Absorption

Two different TEA lasers were used to try to dissociate OCS. The first laser delivered 2 J of energy in 1 μsec and then was focused by using either a 5 or 10 inch focal length lens. The second laser delivered up to 15 Joules in 1 μsec or 3 Joules in less than 100 nsec. In all experiments, the OCS pressure was varied between 0.1 and 3.0 torr. Infrared spectra were taken both before and after irradiation with up to 5,000 pulses. There was no discernible change in the spectrum from before to after excitation. To see if only very small amounts of OCS were dissociated, two cells were simultaneously filled with 1 torr of carbonyl sulfide. One cell was used as a standard while the other was pumped by the laser for 45 minutes (2500 pulses). A quantitative spectral analysis was then done by comparing the signals at masses 60, 48, 34, 32, and 28 corresponding to the masses of OCS, SO, ^{34}S, ^{32}S, and CO, respectively, between the two samples. Again there was no change in the intensity of the mass spectrum showing that no dissociation took place. The possibility remained that small amounts of OCS dissociated to CO and S and then the back reaction of

S + CO → OCS took place showing no change in either the infrared or mass spectrum after irradiation. To ensure that this was not the case, in situ measurements of sulfur particulates was done. A He-Ne laser was set-up colinear to the CO_2 laser light with a photomultiplier tube with a laser filter (6328 Å) monitoring the He-Ne laser. Any formation of particulates should be scattered by the He-Ne laser giving rise to a dip in the photomultiplier signal. Again, nothing was observed. To test for the possibility of the sulfur coming off as excited S_2 radicals and not particulates, a photomultiplier was used to look for the well-known transition of S_2 at 3400 Å. Once again, no product was seen. Other experiments were also done by placing the OCS sample in an oven and heating up to 150°C. This was done in order to populate the upper levels of OCS and then use the CO_2 laser at slightly off-resonance lines to dissociate the molecules. In all cases, no dissociation was observed by all methods of detection. In fact, the only time any dissociation was observed was when the beam was purposely bounced off the glass wall of the cells to form particles and, in effect, facilitate dielectric breakdown. A last experiment was done to check for the possible dissociation of OCS. It is well known that the radiative lifetime of vibrationally excited CO is exceedingly long. In order to see if we did form vibrationally excited CO, an InSb detector was used to view the vibrational fluorescence under the very high excitation conditions. The only fluorescence noted was that which was due to the OCS energy transfer discussed in the previous section. No fluorescence detected could be attributed to CO emission. We finally concluded that, even under the high fluence conditions used (> 100 J/cm^2), the triatomic molecule OCS does not dissociate.

C. Dielectric Breakdown

Earlier experiments[8] have determined that the threshold for dissociating OCS via dielectric breakdown is 20 torr using a 2 Joule CO_2 laser pulse. Furthermore, the products were CO(g) and particulates of sulfur. Our study focused on studying the emission spectrum accompanying the dielectric breakdown of OCS.

In order to discriminate between continuous emission which accompanies the plasma state and the discrete atomic and molecular emission which arise from the molecule of interest, emission spectrum of the dielectric breakdown of various rare gases was also studied. Visible spectra were observed using an optical multichannel analyzer which allowed for single-shot scanning of the entire emission spectrum and also by using a monchromator with a phototube so that the time dependence of individual species could be studied.

Figure 9 shows the laser induced dielectric breakdown spectrum (LIDBS) of 300 torr of He with a one Joule laser pulse. Figure 10 shows the LIDBS spectrum for 225 torr of Ar and Figure 11 is the spectrum of 100 torr of OCS. Each of these spectra were obtained by using the monochromator and phototube.

The identification of the major peaks in the spectrum was accomplished by matching the wavelength against all known lines for the species and states which might be present via a computer program developed by Langsam[26].

In the case of the He, the peaks at 450 nm and 590 nm arise from a He species involving a $^3D \rightarrow {}^3P$ transition[27]. The longer wavelength transition, which is more intense, involves a 1s2p-1s3d transition array and the shorter wavelength peak is the next transition in this

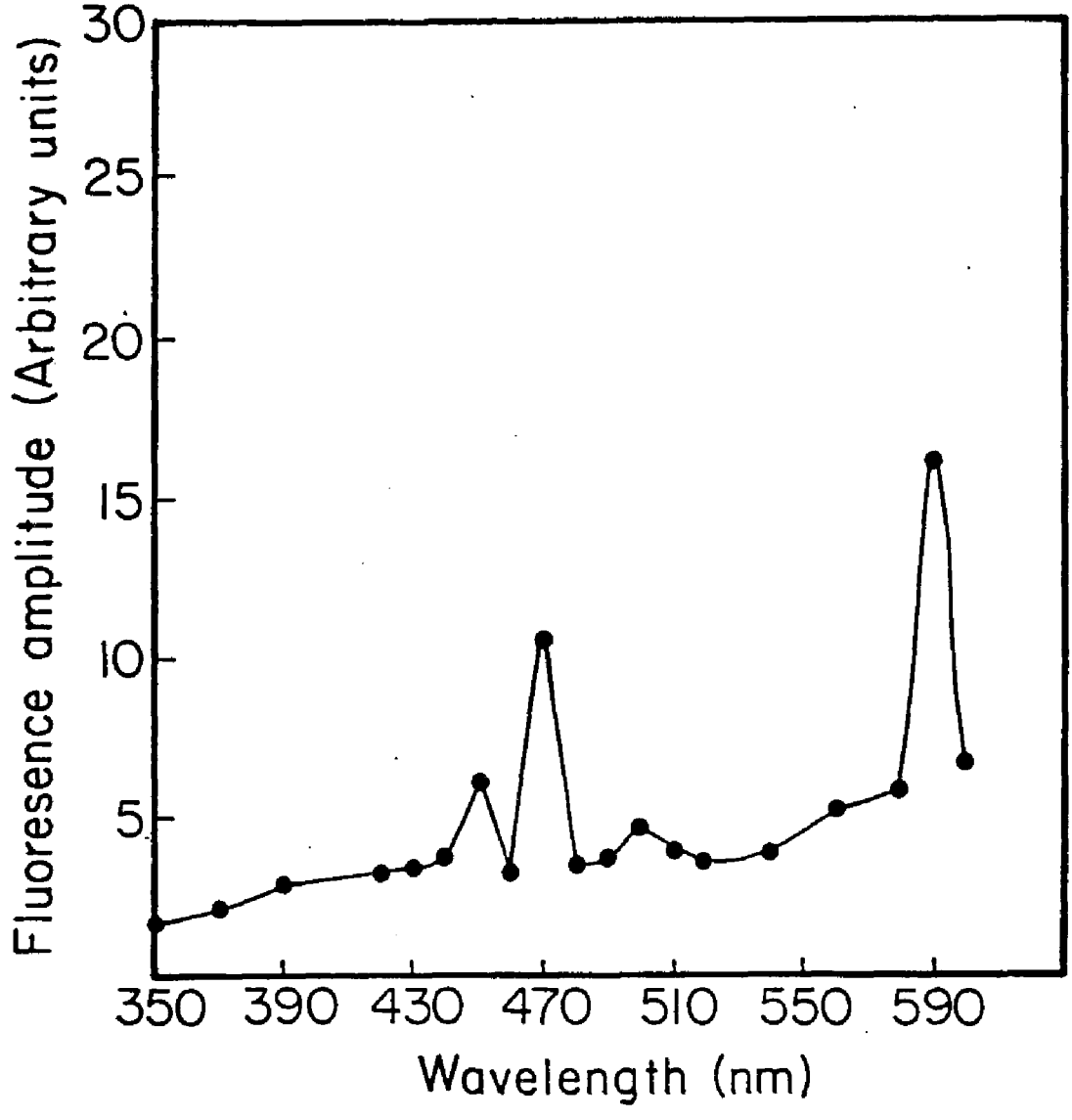

FIGURE 9

LIDBS of Helium

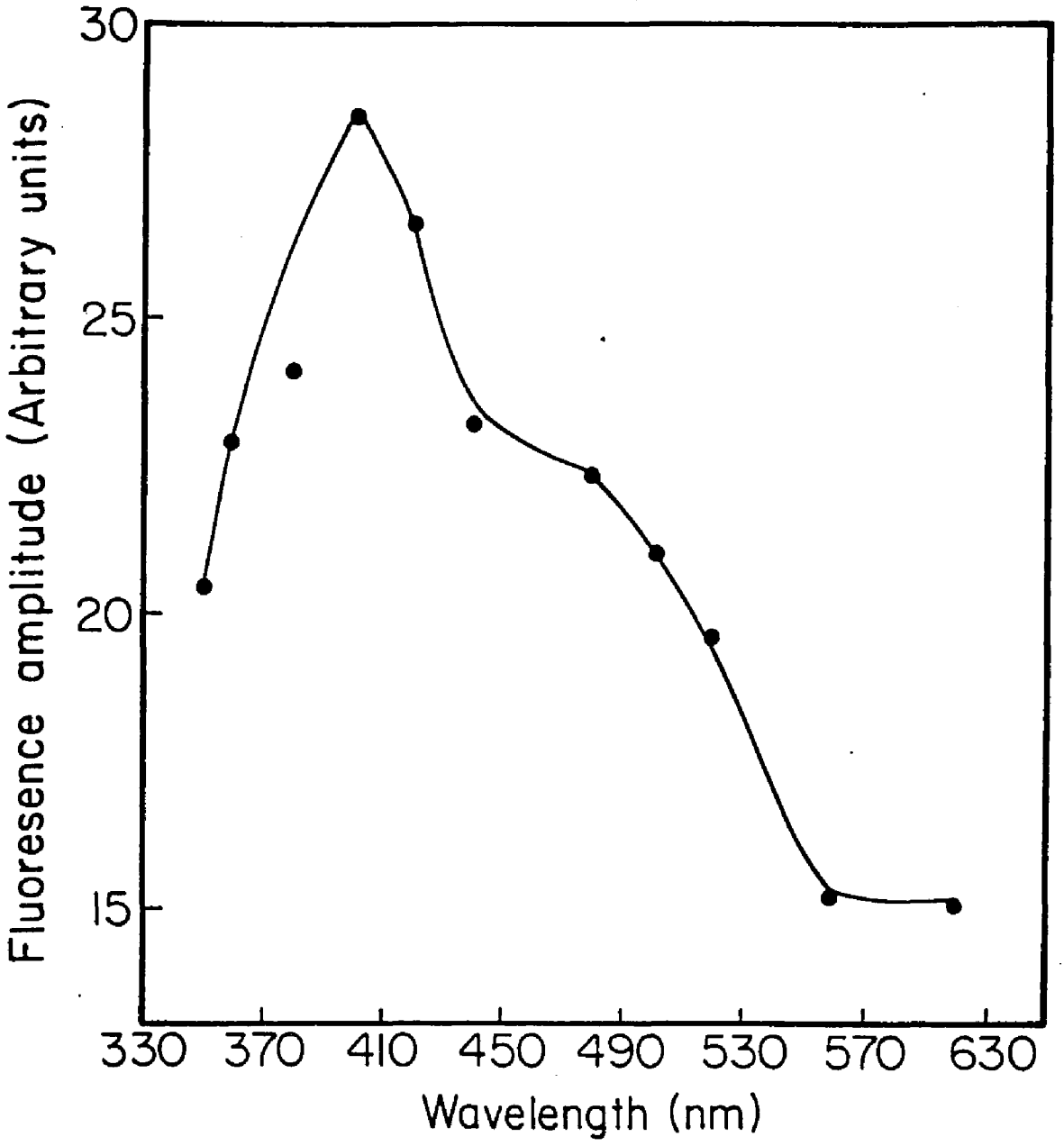

FIGURE 10

LIDBS of Argon

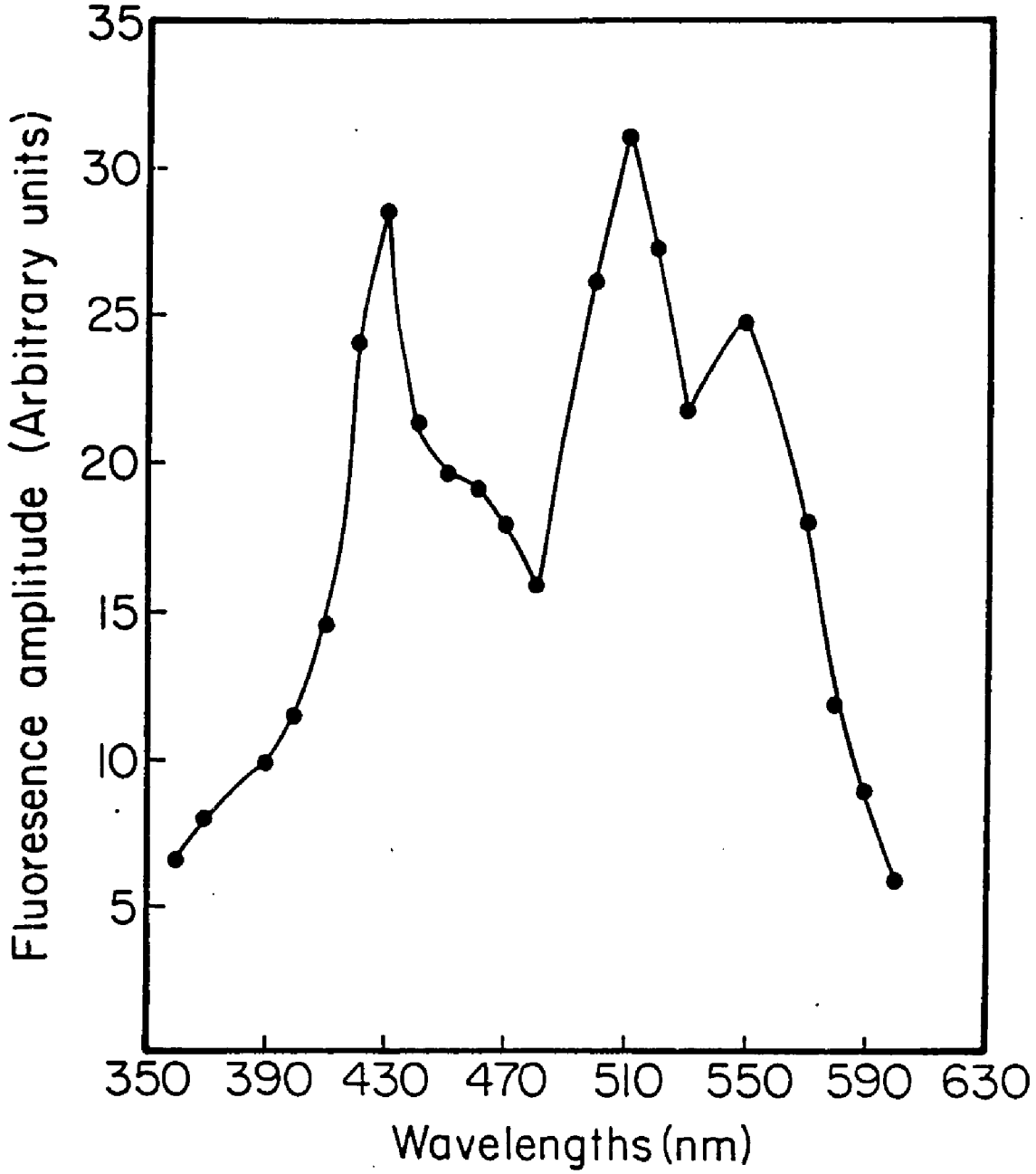

FIGURE 11

LIDBS of OCS

series which corresponds to the 1s2p-1s4d array. Both of these species are relatively long-lived ($\sim$ 20 μs) as compared to the 470 nm emission which involves a He II species and is very short-lived ($\sim$ 2 μs).

The LIDBS of Ar is more intense than He and also shows its greatest intensity at the shorter end of the visible spectrum. Species involving transition from both Ar I and Ar II have been identified.

The OCS spectrum exhibits three major peaks which have been identified. The peak at 430 nm involves a CO transition, the peak at 510 nm is a C_2 transition and, at 550 nm, it is a S II species which is emitting. Within experimental error, all the species were found to occur approximately 50 nsec after the laser pulse. The decay times of the species were slightly different with the S II emission being the fastest ($\sim$ 1.8 μsec) of the three.

In order to obtain a greater understanding of the mechanism of dielectric breakdown, experiments were done to try and differentiate between a shock-wave mechanism and a photodissociation mechanism. Mixtures of OCS with He (.3% and 1%) were photolyzed and their LIDBS was taken. By monitoring the lines at 430 nm, 510 nm, and 550 nm, we tried to ascertain whether the OCS, which we dissociated, as evidenced by the formation of particulates detected by a He-Ne laser, also emitted. In the case of the .3% mixture, the spectrum obtained with the phototube was identical to the LIDBS of pure He. In the 1% mixture, the intensity of the 450 nm peak of He was more intense than the 470 nm peak which may indicate some contribution from the CO emission. However, due to the continuous emission, it was not possible to conclusively say that the OCS was indeed emitting. Similar experiments done with mixtures of OCS and Ar were also inconclusive.

In another experiment, two separate cells separated by a quartz window were filled with 200 torr of Ar and 15 torr of OCS respectively. A laser pulse was passed through the cell containing Ar which was perpendicular to the cell containing OCS and the dissociation of OCS was monitored using a He-Ne laser. After twenty minutes (1,000 pulses), particulates were found in the cell containing OCS. A similar experiment was done using He and OCS and, in this case, no particulates were found even after 2,000 pulses. In fact, this type of behavior is to be expected. In the case of Ar, its LIDBS shows intense lines shifted to the blue as compared to He. Furthermore, the spectrum of Ar in the ultraviolet portion of the electromagnetic spectrum is more intense than that of He. The dissociation energy of OC-S is 3.7 eV[28] which corresponds to 3300 Å. Therefore, the breakdown plasma of Ar is able to photodissociate OCS molecules, while the breakdown plasma of He which is not as intense in the blue can only dissociate OCS via a shock-wave mechanism.

Discussion

A. Energy Transfer

There has been some disagreement over the vibrational energy transfer mechanisms in OCS[29,30]. In a particular wavelength region, the intensity of fluorescence represents the population of molecules in the vibrational energy levels within this region so the rates of activation and deactivation of the fluorescence correspond to the rate of collisional energy transfer into and out of the levels, respectively.

Comparison of Figure 4 to the laser energy used identifies the laser-pumped transition as the bending mode overtone, $0 \rightarrow 2\nu_2$. This energy is then distributed among all other vibrational modes by means of V-V energy transfer. The very fast "up the ladder" transfer within the ν_2 manifold may be described by the reactions

$$OCS(2\nu_2) + OCS(\nu_2) \rightleftarrows OCS(3\nu_2) + OCS(0) + 2\Delta E \qquad (20)$$

$$OCS(3\nu_2) + OCS(\nu_2) \rightleftarrows OCS(4\nu_2) + OCS(0) + 3\Delta E \qquad (21)$$

where ΔE is a small anharmonicity defect. After the ν_2 mode is pumped by the laser pulse, collision can be expected to re-establish vibrational equilibrium by processes such as

$$OCS(2\nu_2) + OCS(0) \rightleftarrows OCS(0) + OCS(\nu_1) + 188\ cm^{-1} \qquad (22)$$

$$OCS(2\nu_2) + OCS(\nu_1) \rightleftarrows OCS(\nu_1 + 2\nu_2) + OCS(0) + 14\ cm^{-1} \qquad (23)$$

$$OCS(\nu_1 + 2\nu_2) + OCS(0) \rightleftarrows OCS(0) + OCS(\nu_3) - 170\ cm^{-1} \qquad (24)$$

$$OCS(4\nu_2) + OCS(0) \rightleftarrows OCS(0) + OCS(\nu_3) + 43\ cm^{-1} \qquad (25)$$

Eventually the excess vibrational energy is converted into translational and rotational energy by V-T/R processes such as

$$OCS(\nu_i) + M \rightleftarrows OCS(0) + M + \Delta E(= E_i) \qquad (26)$$

where M can represent an OCS molecule in any state or a molecule of a different species. The energy deficit here is equal to the energy of the state undergoing deactivation.

In our discussion, we will be interested in the rise of fluorescence at 4.8 μ which may derive from a combination of mechanisms which would fill the ν_3 level. For any mechanism, there are usually two criteria that are given prime consideration. The first of these is the size of the energy deficit, ΔE. As described in the theoretical section, the probability of energy transfer decreases strongly with increasing energy gap. Based on this, a mechanism which may be expected to contribute to the 4.8 μ fluorescence rise would be rapid population increase of $4\nu_2$ via reactions (20) and (21) followed by the intermode crossover from $4\nu_2$ to ν_3 [reaction (25)]. This reaction is energetically favorable since ΔE is 43 cm^{-1}. However, the other important criteria in describing the mechanism is the magnitude of the breathing sphere parameter for the normal modes involved. These parameters function as matrix elements in the expression for energy transfer probability in modified SSH theory. For OCS, the values for the normal modes are[31] $\langle A_1^2 \rangle = 0.020$, $\langle A_2^2 \rangle = 0.0066$ and $\langle A_3^2 \rangle = 0.0091$ all in amu^{-1}. The results of breathing sphere theory predict that the

probability for a transition decreases drastically as the number of vibrational quanta exchanged in the transition increases[12,32]. Therefore, filling of ν_3 by $4\nu_2$ which involves the simultaneous change of one vibrational quantum by one mode (ν_3) and four quanta by another mode (ν_2) might be expected to be improbable. Therefore, it seems as though the OCS system offers a considerable theoretical challenge to the usual energy transfer theories.

In order to explain these discrepancies between theory and experiments, one must look more closely at the OCS system. The $4\nu_2$ and ν_3 states are known to be slightly mixed by Fermi resonance[33]. This mixing leads to a small first order harmonic oscillator matrix element between $4\nu_2$ and the ground state. Therefore, reaction (25) may be thought of as a collision which induces a transition from a state with a small amount of ν_3 character ($4\nu_2$) to a state with a large amount of ν_3 character (00°1). Moreover, the bending modes of OCS exhibit an extremely large electrical anharmonicity[34]. This leads to the fact that the $0 \rightarrow 4\nu_2$ transition has been directly observed in absorption[35] and the derivative of the dipole moment of this band has been measured to be 2% as large as that of the $0 \rightarrow \nu_3$ transition[36]. According to SSH theory, the energy transfer probability is given by equation (1) and (4) of the theoretical section. Using pure harmonic oscillator OCS state for the interaction potential and the breathing sphere parameters mentioned earlier, the probability of filling ν_3 via $4\nu_2$ is eight orders of magnitude too small. However, a more accurate computation of the interaction potential includes the mixing of the OCS levels by mechanical anharmonicities. The levels, $4\nu_2$ and ν_3, mix with nearby levels by Fermi resonances and higher order mixing terms where

$$\Psi_{00^\circ 1} = 0.997|00^\circ 1\rangle + 0.084|02^\circ 0\rangle + 0.002|10^\circ 0\rangle$$

$$\Psi_{04^\circ 0} = 0.948|04^\circ 0\rangle + 0.269|12^\circ 0\rangle + 0.028|20^\circ 0\rangle - 0.167|02^\circ 1\rangle - 0.022|10^\circ 1\rangle + 0.010|00^\circ 2\rangle.$$

Using this interaction potential, Flynn and co-workers[31] have shown that the probability is only one order of magnitude lower than the experimentally determined value.

The results of the focused TEA laser excitation is also consistent with the above explanation. When the beam is focused, fewer molecules are actually excited which explains why the intensity of the fluorescence is weaker than in the unfocused case. Furthermore, since molecules are pumped to even higher states, the risetime for the ν_3 mode is expected to be slower in the focused case. Indeed, our results show a risetime of 23.4 $msec^{-1}torr^{-1}$ under focused conditions as opposed to 53.4 $msec^{-1}torr^{-1}$ for the unfocused case (Table 1).

In conclusion, our energy transfer results of OCS are consistent with those observed by other methods. There does not seem to be any special consideration in terms of the transfer of energy under TEA laser conditions that may help to explain why this molecule would not dissociate under high intensity laser excitation. With this in mind, we now turn to our discussion of the results of the multiple photon excitation of OCS under collisionless conditions.

B. MPD

Before we proceed to our discussion of the lack of multiple photon dissociation of OCS, we must take a careful look at the molecular properties that may influence the absorption and dissociation processes.

These properties include the energy of activation for the reaction, the information necessary to estimate the density of vibrational states, and the low intensity absorption cross-section. The last property in fact depends on the laser frequency and is, therefore, not a molecular property.

Many researchers believe that the density of vibrational states has a greater effect on the multiple-photon-absorption process than most other molecular properties. As discussed earlier, the density of vibrational states defines the quasicontinuum region[37], determines the unimolecular reaction rate in RRKM and other theories[5], and dominates the theory of intermode energy flow[38].

An exact computation of the density of states function for a given molecule requires a large amount of spectroscopic data, such as fundamental vibrational frequencies, anharmonicity constants, and Fermi-resonance parameters. However, very often, much of this data is unavailable.

Approximation methods, such as the Whitten Rabinovitch method[5], are usually used by the laser chemist. This method gives

$$N(E_v) = \frac{(E_v + aE_z)^{S-1}}{(S-1)!\prod_{i=1}^{S} h\nu_i}\left[1 - \beta\frac{dw(E')}{dE'}\right] \qquad (27)$$

for the density of vibrational states, $N(E_v)$, at vibrational energy, E_v, above the ground vibrational state. The quantity, E_z, is the zero-point vibrational energy, S is the number of vibrational degrees of freedom, and the ν_i are the set of fundamental vibrational frequencies. The factor, a, is

$$a = 1 - \beta w(E') \tag{28}$$

where $$\beta = \frac{S-1}{S} \cdot \frac{\langle \nu^2 \rangle}{\langle \nu \rangle^2} \tag{29}$$

and the empirical function w(E') is

$$w(E') = (5.00\ E' + 2.75\ E'^{0.5} + 3.51)^{-1} \quad (0.1 < E' < 1.0)$$

$$w(E') = \exp(-2.4191\ E'^{0.25}) \quad (E' > 1.0) \tag{30}$$

and $$E' = E_v/E_z. \tag{31}$$

This approximation method requires four parameters for each species: the arithemetic mean of the fundamental vibrational frequencies, the geometrical mean of the fundamental vibrational frequencies, $\bar{\nu}$, the number of vibrational degrees of freedom, S, and the frequency spread parameter, β. Equation (27) then becomes

$$N(E') = \frac{2(\frac{S\langle \nu \rangle}{2\bar{\nu}})^5 (E'+a)^{S-1}}{S!h\langle \nu \rangle} \left[1 - \beta \frac{dw(E')}{dE'}\right] \tag{32}$$

Another molecular property that most certainly plays a major role in determining the probability of reaction for a given laser energy fluence is the energy required to promote the reaction. For a simple dissociation reaction, such as dissociation of OCS to CO and S, that energy is very nearly the bond strength for the observed reaction. For more complex reactions, such as elimination of a diatomic molecule from an ethane derivative, the activation energy may exceed the

the enthalpy change for the reaction by a substantial amount.

Table 2 lists the quantities necessary to calculate the vibrational density of states function from the Whitten-Rabinovitch method for OCS which does not undergo dissociation, and for SF_6 and BCl_3 which are known to dissociate via MPD[2,39]. The table also lists the density of vibrational states at E_v = 10500 cm^{-1} (~ 11 CO_2 photons) and activation energy for each of the molecules. We can see that the density of vibrational states depend very strongly on the number of atoms in the molecule or on the number of vibrational degrees of freedom.

A short review of the general physical picture for MPD is now in order. As described earlier, the excitation can be divided into a region where the molecular energy states are discrete and to a second region where the states are in a quasicontinuum. The onset of region II is essentially determined by the size of the molecule, i.e., the number of atoms, as well as by the excess vibrational energy. Obviously, for a diatomic molecule, region II does not exist. For triatomics, it is an open question whether region II exists at all and, in any case, region I will contain a large number of levels, and the properties of this region will dominate the characteristics of the multiphoton excitation process. In order to excite the molecule over the discrete states with high probability, the infrared laser field must be sufficiently intense and near the resonance of a vibrational mode. The near-resonance condition implies that this excitation step can be isotopically selective as long as the isotope shift is comparable to the absorption bandwidth. Rotational energy compensation of vibrational anharmonicity in the first few transitions is effective in bringing the excitation close to resonance. Perfect matching of the laser frequency

Table 2

Species	E_a(kcal)	<v>	$\tilde{\nu}$	β	N(10500)	Ref[a]
OCS	73.3	1,149	976	0.89	8.02×10^1	40,40
BCl_3	105	567	483	1.08	1.75×10^5	40,40
SF_6	92.6	624	591	1.03	8.5×10^8	41,42

[a] First Ref is E_a source and second is fundamental vibrational frequency source.

with the fundamental frequency of the vibrational mode is not necessary, because of power broadening and the spread of initial population over many rotational states and in the excited vibrational manifold even with molecules at room temperature. With a sufficiently intense laser beam, molecules have been observed to dissociate even when excited on relatively weak combination bands[43].

Once the molecule is excited over the discrete states and into the quasicontinuum, the subsequent multiphoton excitation to and beyond the dissociation level is essentially composed of successive resonant steps. The average level of excitation of the molecules is then proportional to the laser energy fluence, rather than the laser intensity. The laser energy deposited in a particular vibrational mode of the molecule is randomized quickly to the other modes. At sufficiently high excitation levels, the redistribution time is on the order of 30 picoseconds[44].

The dissociation process that follows can be well described by the RRKM theory for unimolecular dissociation which assumes complete energy randomization.

From the above discussion, we can make a number of assertions regarding the multiple-photon dissociation process. On the laser pulse requirement, the leading part of the pulse must be intense enough to excite the molecule over the discrete states into the quasicontinuum and the remaining portion of the pulse must contain enough energy fluence to excite the molecule beyond the dissociation limit. If the laser intensity required for excitation over the discrete states is much smaller than the peak intensity of the laser pulse, then the dissociation yield is a function of the laser fluence

and not the laser intensity. For smaller and lighter molecules, the quasicontinuum states effectively begin at higher energies. Therefore, for otherwise equal initial excitation conditions, it will take a larger number of photons and, therefore, a higher laser intensity to excite a smaller and lighter molecule over the discrete states. For example, if we compare the fluence needed to give a 1% reaction probability for SF_6 and C_2H_4, we find that, for SF_6, fluence is ~ 1 J/cm^2[45] while, in the lighter C_2H_4 molecules, fluences on the order of 50 J/cm^2[46] are needed. In the case of BCl_3, which has less atoms than C_2H_4 but is heavier, 29 J/cm^2 are needed[39].

Using the above discussion as a guide, we now proceed to our discussion of the MPD of carbonyl sulfide. The dissociation energy of OCS as seen from Table 2 is 73.3 kcal. The laser frequency used is the P(22) 9.6 line of the CO_2 laser which corresponds to an energy of 2.3 kcal. Therefore, 30 photons are necessary to decompose the OCS molecule. From Table 2, we also see that at a vibrational energy 10,500 cm^{-1} above the ground state, the density of states is only in the range of 80/cm^{-1}. Using equation (32), we can calculate that, even at 30,000 cm^{-1}, which is near the dissociation limit, there are still only approximately 300 states per cm^{-1}. Obviously, given this rather small density of states and the need for 30 photons, we would expect that very high laser intensities would be necessary to dissociate OCS via MPD.

Other factors which must be considered include the fact that the pumped mode in OCS is an overtone of the bending mode. In many molecules, this fact would tend to rule out the possibility of absorbing enough energy to dissociate it via MPD. However, in the case

of OCS, the absorption strength of the fundamental $0 \rightarrow \nu_2$ and overtone $0 \rightarrow 2\nu_2$ transitions are nearly equal. This allows substantial energy to be pumped into the overtone transition by the CO_2 laser.

The other points which must be discussed regarding OCS dissociation include the anharmonic shift of the pumped vibrational manifold and the power broadening which may compensate for this anharmonicity. Foord, et al report a calculated anharmonic shift of approximately 0.1 cm^{-1}[47]. For our experimental conditions using either the long pulse laser having an energy of 10 J in 1.5 μsec or the short pulse with 2 J in 100 nsec, the laser intensity is on the order of 10^9 w/cm^2. Using equation (15), we calculate that, at this laser intensity, the power broadening is on the order of 0.3 cm^{-1}. Since the MPD of OCS must be described in terms of a quasi-resonant multiphoton excitation, the power broadening should be large enough to compensate for the calculated anharmonicity. However, Maki, et al[35] report a measured anharmonicity of 35 cm^{-1} for the $6\nu_2$ state, which corresponds to three laser photons. This large anharmonicity obviously could not be overcome by the power broadening.

In light of the above discussion, we can now understand why we were unable to detect any dissociation of carbonyl sulfide. Since OCS is a triatomic molecule having a very low density of states, its multiple photon absorption characteristics are governed by region I effects, that is by discrete energy levels. In order to excite the molecule to its dissociation limit, laser intensities on the order of 10^{15} W/cm^2 or higher would probably be necessary.

Before we can conclude our discussion, we must take note of the report by Proch and Schroeder[48] that they have dissociated OCS in a

molecular beam. They also report the dissociation of ozone, another triatomic molecule. The experimental set-up involved measuring the intensity of the molecular beam with a scaler coupled to a data processing unit. If the molecule dissociates when the CO_2 laser is passed perpendicular to the beam, a dip in the counting rate is observed. They report that the threshold power necessary for dissociation is 1.3×10^8 W/cm^2.

In light of our results and discussion, it is difficult to understand the results of Proch and Schroeder. Our experimental conditions only differed from theirs in the method of detection. Unfortunately, we do not have a molecular beam-mass spectrometer system to repeat their experiments and confirm their results. Their report does not address itself to the theoretical difficulties encountered in trying to explain the phenomenon they observe.

The only possible explanation for the difference in results may be the possibility of a back reaction of CO and S in our system. However, even under flow conditions, we did not detect any formation of sulfur with a He-Ne laser.

In conclusion, we report that we are unable to dissociate OCS using laser intensities on the order of 10^9 W/cm^2 and fluences in the range of 100 J/cm^2. No infrared or electronic fluorescence can be detected from any possible product. We feel that, with the CO_2 lasers presently available in typical university laboratories, the only way to dissociate a triatomic molecule is via dielectric breakdown which is consistent with the theoretical framework of multiple-photon dissociation.

C. Dielectric Breakdown

Laser induced chemical reactions under plasma conditions belong to the high temperature category and are, therefore, thermodynamically

controlled. The plasma can be differentiated into two regions, the small dense core dominated by ionic species and the less dense region dominated by free radicals and atoms. Ions have very short lifetimes so that chemical processes occurring in this region can be ignored. Most of the chemistry would be expected to take place outside the core.

The cold gas molecules surrounding the outside of the plasma act as quenching agents and also prevent the free movement of the highly excited specie produced inside the plasma.

Extensive studies have shown[25] that laser induced dielectric breakdown of almost any hydrocarbon yields C_2H_2 as a major product and eventually the exclusive product as irradiation proceeds. This result has been attributed to the conditions of high temperature and fast quenching rate. This indicates that the characteristics of the LIDB reaction is short reaction time, high temperature, and rapid quenching. Moreover, the product formation of laser induced reactions, either by multiphoton absorption processes or via gas breakdown, always show the same results.

In a simple system such as OCS, it is quite clear that the weakest bond in the system is the C-S bond, and one would, therefore, expect the products of OCS dissociation to be CO(g) and sulfur particulates. In fact, particulate formation is very substantial and easily observable. Decomposition of a 60 torr sample of OCS in the presence of 150 torr of Ar was carried to completion in 3200 pulses. The photon utilization factor, defined as the number of photons injected into the sample divided by the total number of molecules dissociated, is equal to 350.

The fact that we can extend the phenomenon of dielectric breakdown to induce reaction of a gas even below its breakdown pressure by

inducing a plasma in a carrier gas leads to some interesting possible applications of LIDB. If one envisions a system containing air and a small percentage of some unwanted gas (e.g., H_2S, SO_2), it should be possible to induce a plasma in the air and still dissociate the gaseous impurity. Our experimental observations show that we can, indeed, do just that. When we irradiated a mixture of 1 torr OCS with 300 torr of He or Ar, particulates were observed throughout the cell indicating that the OCS had been dissociated even though its pressure was well below the pressure needed to induce DB in pure OCS.

Furthermore, by studying the LIDBS of the species involved, one can gain a better understanding of the mechanism of this dissociation. In the case where He was the carrier gas, the dissociation observed outside the focal point area must be ascribed to a shock-wave mechanism. This is proven by the fact that particulates are observed throughout the cell, even though the plasma light cannot induce photodissociation when a quartz window is inserted between the gases. This is due to the fact that, in order to photodissociate OCS, light of wavelengths shorter than 3300 Å is necessary[28]. Since the LIDBS of He does not have any significant intensity in the ultraviolet portion of the spectrum photodissociation cannot occur.

However, in the case of the Ar/OCS mixtures, both a shock-wave and photodissociation mechanism account for the particulate formation. This is proven by the detection of particulates in the cell containing OCS separated by a quartz window from the plasma induced in the Ar. This can be explained by noting that the LIDBS of Ar has significant intensity at shorter wavelengths which can photodissociate OCS.

Another important area of application of LIDB revolves around the optical emission which accompanies the breakdown process. The emission

processes in a plasma may be briefly summarized as follows:

i) Bound-Bound Transitions. The energy of a photon emitted as an atom or ion makes a transition from one bound state to another of lower energy gives rise to a spectral line which is well defined and whose profile depends on the spontaneous lifetime of the upper state as well as the velocity distribution of the emitting atoms. Collisions and the presence of external electromagnetic fields may all perturb the initial and final states of the emitting atom of molecule. A cool partially ionized gas possesses line radiation in the infrared-visible region of the spectrum. At higher temperatures, the atoms can be raised to more energetic excited states and emit lines of shorter wavelengths.

ii) Free-Bound Transition. A free electron may be captured by an ionized atom upon which the surplus energy will be emitted as a photon. Given a particular final bound state, the emission spectrum for a recombination process is a continuum with a sharp low-frequency cut-off. The cut-off point, known as the recombination limit, corresponds to the ionization potential of the final bound state. If two electrons collide with an ion simultaneously, one may be captured while the other carries away the surplus energy without the emission of radiation. This three body recombination becomes more probable as the electron density rises.

iii) Free-Free Transitions. A free electron colliding with another particle will make a transition to another free state of lower energy accompanied by the emission of a photon. This radiation is known as Bremsstrahlung and forms a continuum. Of more importance is the inverse process, known as "inverse Bremsstrahlung," in which an electron absorbs a photon as it moves from one free state to a more energetic one. As

we discussed earlier, this is the primary process by which laser induced dielectric breakdown takes place.

In the case of this laser induced plasma, measurements of the spectral distribution of the plasma emission indicate a strong line spectrum superimposed on a continuum which peaks at characteristic wavelengths depending on the plasma medium. Spectral analysis of the plasma allows one to detect the atomic (ionic and neutral) constituents of the gas molecules. By applying this technique to mixtures of gases, one should, in principle, be able to detect small quantities of a particular material in a host gas. By obtaining the breakdown spectrum of the gas of interest and also of the carrier gas and monitoring a specific wavelength, one can use this technique for the confirmation of the presence of a particular material in a mixture. This technique should be specifically useful to probing hostile environments since it is an optical process not a physical one.

In the following chapter, we will describe the application of this technique more fully. In the OCS/rare gas mixtures using a photomultiplier, we were unable to conclusively identify spectral lines due to OCS. We feel that the reason for this is due to the detection techniques. As we will see in our next chapter, when we used an Optical Multichannel Analyzer to detect the plasma emission, we were able to easily identify emissions of the impurity gas at 2 to 3% concentrations. With better signal averaging, we strongly believe that this technique can also be applied successfully using a photomultiplier-monchromator arrangement which would allow for real-time detection of impurities in a gaseous mixture.

Conclusion

Our studies of the CO_2 laser reactions of carbonyl sulfide under both high and low excitation conditions has yielded very interesting results. The energy transfer study gives us important information regarding the different pathways the OCS molecule dissipates its energy upon collisions and we were able to understand these results by using the existing theoretical models for such processes. The fact that we were unable to dissociate OCS via multiple-photon dissociation was very disappointing, though this too can be understood in light of the high intensities which are necessary to dissociate a triatomic molecule. Finally, our study of the dielectric breakdown of OCS and the emission spectrum accompanying it gained us a greater understanding of the LIDB process and some of its potential uses.

Bibliography for Chapter 1

1. E. Weitz and G. W. Flynn, Ann. Rev. Phys. Chem., 1974, 25, 275.

2. C. P. Robinson, Annals of the New York Academy of Sciences, 1976, 267, 81.

3. E. Fuss and T. P. Cotter, Appl. Phys., 1977, 12, 265.

4. A. S. Sudbo, P. A. Shulz, E. R. Grant, Y. R. Shen, and Y. T. Lee, J. Chem. Phys., 1979, 70, 912.

5. P. J. Robinson and K. A. Holbrook, "Unimolecular Reactions," Wiley, New York (1972).

6. R. P. Karl and J. L. Lyman, J. Chem. Phys., 1978, 69, 1196.

7. J. L. Lyman, G. P. Quigley, and O. P. Judd, "Multiple Photon Excitation and Dissociation of Polyatomic Molecules," Springer-Verlag, Heidelberg, West Germany (1980).

8. A. M. Ronn, Chem. Phys. Lett., 1976, 42, 202.

9. A. Foord and D. H. Whiffen, Mol. Phys., 1972, 26, 959.

10. A. G. Maki and S. H. Freund, J. Mol. Spectros, 1976, 62, 90.

11. R. N. Schwartz and K. F. Herzfeld, J. Chem. Phys., 1954, 22, 767.

12. F. L. Tanczos, J. Chem. Phys., 1956, 25, 439.

13. M. J. Coggiola, P. A. Schulz, Y. T. Lee, and Y. R. Shen, Phys. Rev. Lett., 1977, 38, 17.

14. P. Kolodner, C. Winterfeld, and E. Yablonovitch, Opt. Comm., 1977, 20, 119.

15. S. Mukamel and J. Jortner, J. Chem. Phys., 1976, 65, 5204.

16. N. Bloembergen, Opt. Comm., 1975, 15, 416.

17. J. P. Aldridge, J. H. Birley, C. D. Cantrell, and D. C. Cartwright, "Laser Photochemistry," Addison Wesley, Reading, Mass. (1977).

18. J. G. Black, E. Yablonovitch, N. Bloembergen, and S. Mukamel, Phys. Rev. Lett., 1977, 38, 1131.

19. R. V. Ambartzumian and V. S. Letokhov, Acc. Chem. Res., 1977, 10, 61.

20. J. G. Black, P. Kolodner, M. J. Schulz, E. Yablonovitch, and N. Bloembergen, Phys. Rev. A, 1979, 19, 704.

21. J. P. Wright, Proc. Phys. Soc., 1964, 84, 41.

22. H. Hora, "Laser Plasma and Nuclear Energy," Plenum, New York (1975).

23. E. Yablonovitch, Phys. Rev. Lett., 1972, 28, 85.

24. J. C. Smith, J. Appl. Phys., 1970, 41, 4501.

25. S. T. Lin, Ph.D. Dissertation, City University of New York, 1978.

26. Y. Langsam, Ph.D. Dissertation, Polytechnic Institute of New York, 1979.

27. W. L. Wiese, M. W. Smith, and B. M. Glennon, "Atomic Transition Probabilities--Hydrogen Through Neon," NSRD-NBS 4, Vol. I, U. S. Government Printing Office, 1966.

28. G. Herzberg, "Molecular Spectra and Molecular Structure," Vol. III, Van Nostrand, 1966.

29. B. M. Hopkins, A. Boronavski, and H. L. Chen, J. Chem. Phys., 1973, 59, 836.

30. J. K. Hancock, D. F. Starr, and W. H. Green, J. Chem. Phys., 1974, 61, 3017.

31. D. R. Siebert and G. W. Flynn, J. Chem. Phys., 1976, 64, 4973.

32. J. L. Stretton, Trans. Faraday Soc., 1965, 61, 1053.

33. Y. Morino and T. Nakagawa, J. Mol. Spectrosc., 1968, 26, 496.

34. J. Braslowsky and Y. Ben Aryeh, J. Mol. Spectrosc., 1969, 30, 116.

35. A. G. Maki, E. K. Plyler, and E. D. Tidwell, J. Res. Nat'l Bur. Stand. Ser. A66, 1962, 163.

36. M. Lev-On, W. E. Palke, and R. C. Millikan, Int. J. Chem. Kinet., 1973, 5, 753.

37. N. Bloembergen and E. Yablonovitch, Physics Today, 1978, 31, No. 5, 23.

38. M. F. Goodman, J. Stone and D. A. Dows, J. Chem. Phys., 1976, 65, 5052.

39. J. L. Lyman and S. D. Rockwood, J. Appl. Phys., 1976, 47, 595.

40. D. R. Stul and H. Prohet, JANAF Thermochemical Tables, Nat'l Bur. of Standards, Wash., D. C., 1971, 2nd Ed.

41. S. W. Benson, Chem. Rev., 1978, 78, 23.

42. R. S. McDowell, J. P. Aldridge, and R. C. Holland, J. Phys. Chem., 1976, 80, 1203.

43. R. V. Ambartzumian, Y. A. Gorokhov, U. S. Letokhov, G. N. Markarov, and A. A. Puretzky, Phys. Lett. A, 1976, 56, 183.

44. H. S. Kwok and E. Yablonovitch, Phys. Rev. Lett., 1978, 41, 745.

45. F. Brunner and D. Proch, J. Chem. Phys., 1978, 68, 4936.

46. J. H. Hall, M. L. Lesiecki, and W. H. Guillory, J. Chem. Phys., 1978, 68, 2247.

47. A. Foord, J. G. Smith, and D. H. Whitten, Mol. Phys., 1975, 29, 1685.

48. D. Proch and H. Schroeder, Chem. Phys. Lett., 1979, 61, 426.

CHAPTER 2

Laser Induced Dielectric Breakdown - Spectra Identification

INTRODUCTION

Atomic absorption spectrophotometry in a variety of forms has been used for the identification of atomic and molecular species. In this chapter, we shall describe a new variant of this technique by using a CO_2 laser to initiate a plasma in a gas. By studying the visible emission spectrum accompanying the plasma, we shall show the feasibility of identifying the atomic, ionic, and molecular species in the plasma and, in effect, "fingerprint" the gas in question. The unique emission spectrum of each individual gas will allow us to apply this technique to a mixture of gases and help identify impurities contained in the mixture. Since this is an optical technique and not a physical one, it should be most useful in probing hostile environments where physical access may not be possible or convenient or when real time measurements are preferred.

We have studied the Laser Induced Dielectric Breakdown Spectrum (LIDBS) of a series of hydrocarbons, methyl halides, fluoromethanes, and chloromethanes. This series of gases were chosen for numerous reasons. Firstly, the reactions of these species under laser excitation have been extensively studied both in terms of their energy transfer mechanism under low-power excitation and product formation when a non-resonant frequency was used as the exciting source. Furthermore, many of these molecules are important in combustion studies as well as to environmental studies.

EXPERIMENTAL

The basic experimental arrangement was similar to that described in Chapter 1. All gases were research grade (Matheson) and were further purified by vacuum distillation. In all cases, a 123 cm^3 square cell fitted with "O" ring mounted NaCl windows was used.

The visible emission was studied using an Optical Multichannel Analyzer (OMA). This system, on loan from the Princeton Applied Research Corporation, consists of a 1250A console, 1250D SIT intensified photomultiplier detector, and a 1208 polychromator which is a specially modified Jarrel Ash .25 meter monochromator. The OMA is a modular electro-optical signal processing system. Optical signals are detected on the target of an image tube which is divided into 500 detection channels. Data may be enhanced by integration over several laser pulses, followed by background subtraction of interfering signals. The spectrum is then displayed on an oscilloscope, photographed, or traced on an X-Y recorder for analysis. Each of the 500 OMA channels was approximately 6 Ångstroms wide as determined by calibration with the 4350, 5461, and 5770 Å Hg lines. A particular channel was set to a known mercury line by means of a monochromator so that the complete visible spectrum between 3093-6003 Å and 4164-7164 Å could be scanned with only two laser pulses. The spectrum is then compared to known tabulated transitions for the species involved by means of a computer program.

Each spectrum was obtained using a fresh sample of gas because it was found that the visible emission of the plasma differed markedly after as few as 10 laser pulses.

RESULTS AND DISCUSSION

Figure 1 shows a typical OMA photograph of the emission spectra of CH_3F, CH_2F_2, CH_3Cl, and CH_3Br. Each individual dot represents a channel which corresponds to a specific wavelength. As is clearly evident, each gas has peaks at a different wavelength which can be ascribed to either an ionic, neutral, or molecular fragment of the parent molecule.

In the following tables, we have tabulated the wavelengths of each spectrum and the probable emitter for each of the species studied[1-7]. If one compares the species in the fluoromethane series, one notices new peaks due to molecular fragments such as CF_2 and CF_3 which begin to appear as the number of F atoms in the series are increased. Furthermore, the intensity of the lines which are identified as emission of F atoms increase as one proceeds from methyl fluoride to carbon tetrafluoride.

The same type of results are noted for the chloromethane series. As the number of chlorine atoms are increased in a CH_xCl_y sample, new bands due to CCl_2 and CCl_3 fragments are identified and the intensity of Cl lines are increased as we proceed from methyl chloride to carbon tetrachloride.

Figures 2 and 3 show the OMA plot of the visible spectrum of CH_4 and CCl_4 respectively in the region 4164-7164 Å. Figure 4 is the spectrum obtained when a mixture of 1 torr CCl_4 and 32 torr CH_4 are irradiated with a laser pulse. Comparison of Figure 4 with Figures 2 and 3 shows that the spectrum of the mixtures contains features of both the methane plasma and that of the carbon tetrachloride. Peaks which are unique to the CCl_4 spectrum are clearly observable

even though the CCl_4 pressure is many torr below the pressure necessary to induce breakdown in pure CCl_4. This proves that we can detect impurities in a gaseous mixture by studying the emission spectrum of the individual components of the mixture and choosing wavelengths where one species emits and not the other.

Figure 5 shows the LIDBS of CF_4 and Figure 6 shows a similar spectrum for a mixture of 3 torr CH_4 with 65 torr of CF_4. Again, by comparing figures 2 and 5 with Figure 6, we see features of both the LIDBS of both pure CH_4 and CH_4 in the LIDBS of the mixture.

Similarly, Figure 7 gives the LIDBS of C_2H_6 and Figure 8 the LIDBS of a mixture of 3 torr C_2H_6 and 65 torr CF_4. By again comparing these figures with that of Figure 5, we note emission which is unique to each indivdual component of the mixture.

In Figures 9, 10, and 11, we show the LIDBS of each of the individual components of the mixture together wtih the LIDBS of the mixture clearly showing that peaks due to each individual gas are apparent in the mixture.

CH_3F

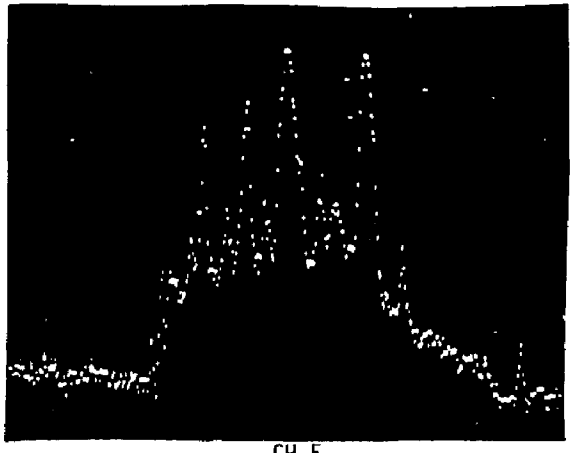

CH_2F_2

CH_3Cl

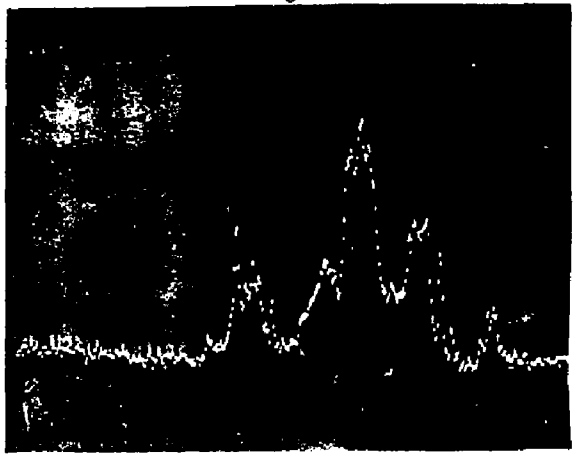

CH_3Br

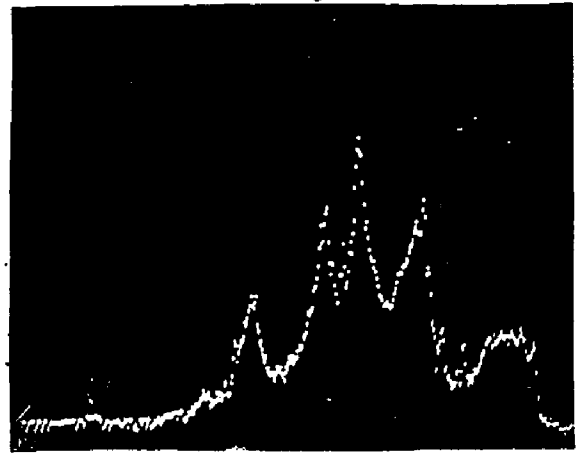

FIGURE 1 - OMA Photograph of CH_3F, CH_2F_2, CH_3Cl, & CH_3Br

Table 1

60 torr CH_4

Wavelength (Å)	Probable Species
4309	CH
4326	CH
4361	C_2
4669	C_2
4843	H_β
5128	C_2
5158	C_2
6598	H_α

Table 2

50 torr C_2H_6

Wavelength (Å)	Probable Species
4332	CH
4355	C_2
4396	C_2
4686	C_2
4838	H_β
5134	C_2
5152	C_2
5545	C_2
5575	C_2
5636	C_2
6610	H_α

Table 3

65 torr CH_3F

Wavelength (Å)	Probable Species
4326	CH
4350	CH
4379	C_2
4681	C_2
4716	C_2
4843	H_β
5140	C_2
5170	C_2
5539	C_2
5557	C_2
5600	C_2
5648	C_2
6622	H_α
6967	F
7021	F

Table 4

40 torr CH_3Cl

Wavelength (Å)	Probable Species
4332	CH
4657	C_2
4681	C_2
4861	H_β
4904	Cl
5104	Cl
5164	C_2
5225	Cl
5436	Cl
5642	C_2
6610	H_α

Table 5

40 torr CH_3Br

Wavelength (Å)	Probable Species
4355	Br
4530	Br
4594	Br
4605	Br
4686	C_2
4856	H_β
5164	C_2
5243	Br
5557	C_2
5594	C_2
5642	C_2
6616	H_α

Table 6

50 torr CH_3I

Wavelength (Å)	Probable Species
4670	I_2
4867	H_β
5057	I_2
5134	C_2
5169	C_2
5223	I_2
5313	I
5348	I
5472	I
5627	C_2
5686	I
5740	I
5781	I
5954	I
6084	I
6286	I
6589	H_α

Table 7

40 torr CH_2F_2

Wavelength (Å)	Probable Species
4320	CH
4350	CH
4682	C_2
4858	H_β
5152	C_2
6271	F
6386	F
6453	F
6622	H_α
6858	F
6955	F
7015	F

Table 8

50 torr CF_3H

Wavelength (Å)	Probable Species
4344	CH
4681	C_2
4868	H_β
5134	C_2
5176	C_2
6041	CF_3
6277	F
6392	F
6459	F
6622	H_α
6864	F
6967	F
7027	F

Table 9

65 torr CF_4

Wavelength (Å)	Probable Species
4431	CF_3
4681	C_2
5134	C_2
5170	C_2
5981	CF_3
6041	CF_3
6114	CF_3
6265	F
6386	F
6447	F
6846	F
6949	F
7009	F
7173	F

Table 10

40 torr CH_2Cl_2

Wavelength (Å)	Probable Species
4338	CH
4350	CH
4640	C_2
4669	C_2
4692	C_2
4797	Cl
4849	H_β
4878	Cl
4908	Cl
5146	Cl
5134	C_2
5169	C_2
5223	Cl
5431	Cl
5455	Cl
5633	C_2
6595	H_α

Table 11

40 torr $CHCl_3$

Wavelength (Å)	Probable Species
4373	Cl
4669	C_2
4678	C_2
4779	Cl
4797	Cl
4849	H_β
4914	Cl
5110	Cl
5134	C_2
5175	C_2
5235	Cl
5288	Cl
5401	Cl
5437	Cl
5455	Cl
5466	Cl
6060	CCl_3
6601	H_α

Table 12

40 torr CCl_4

Wavelength (Å)	Probable Species
4367	Cl
4657	C_2
4779	Cl
4797	Cl
4884	Cl
4901	Cl
5098	Cl
5110	Cl
5134	C_2
5169	C_2
5229	Cl
6150	CCl_3
6304	CCl_3

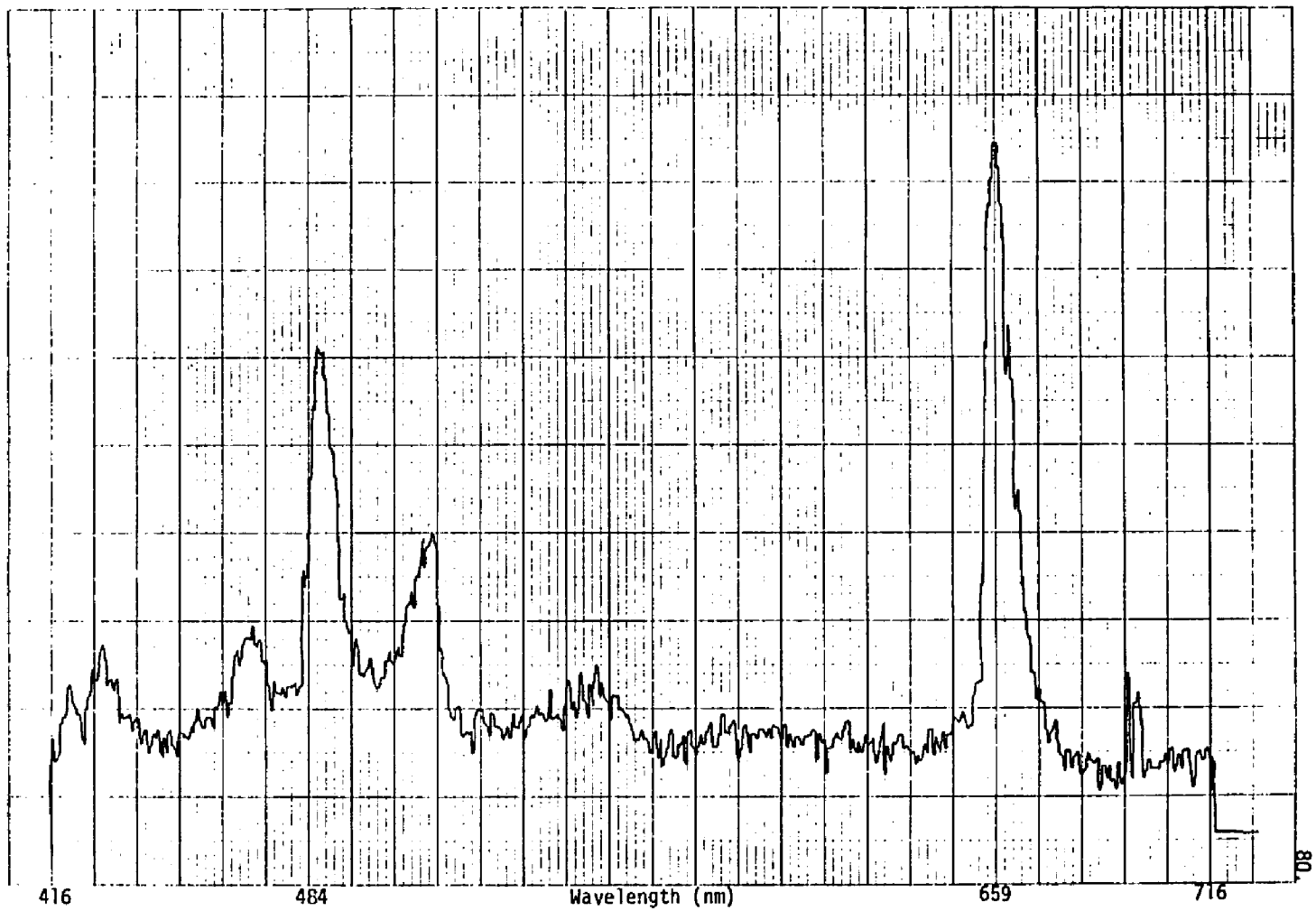

FIGURE 2 - LIDRS of CH_4

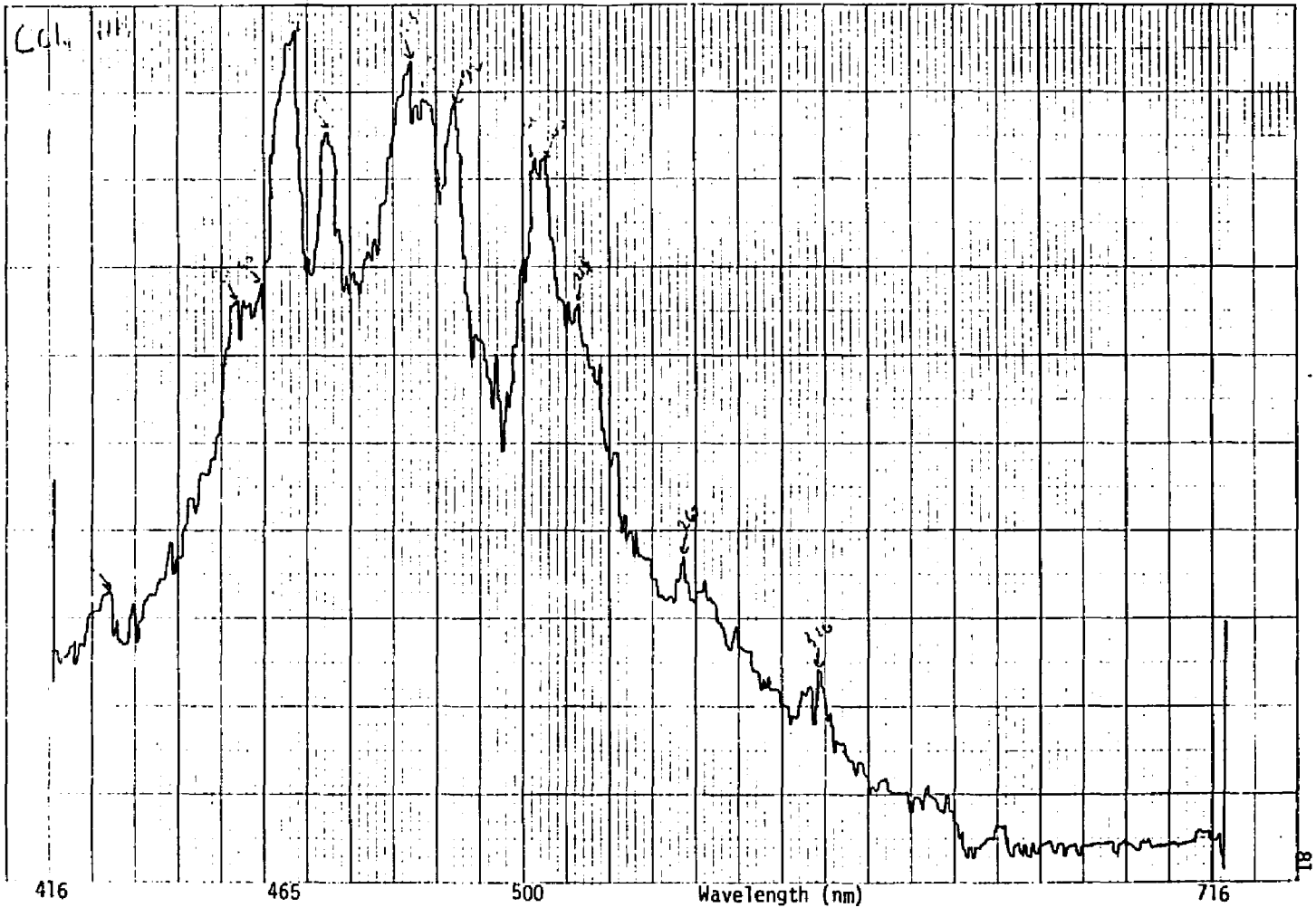

FIGURE 3 - LIDBS of CCl_4

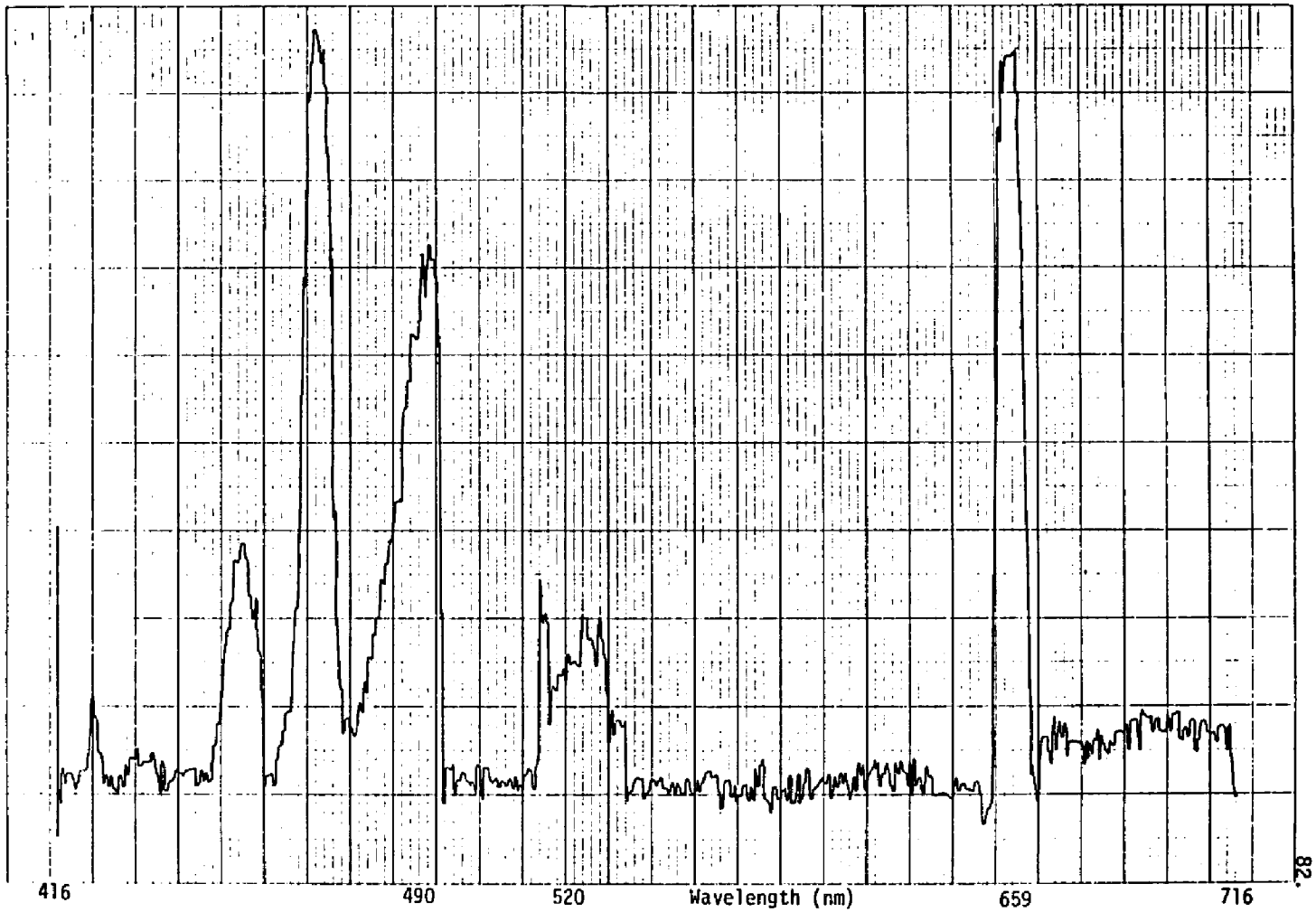

FIGURE 4 - LIDBS of CCl_4/CH_4 Mixture

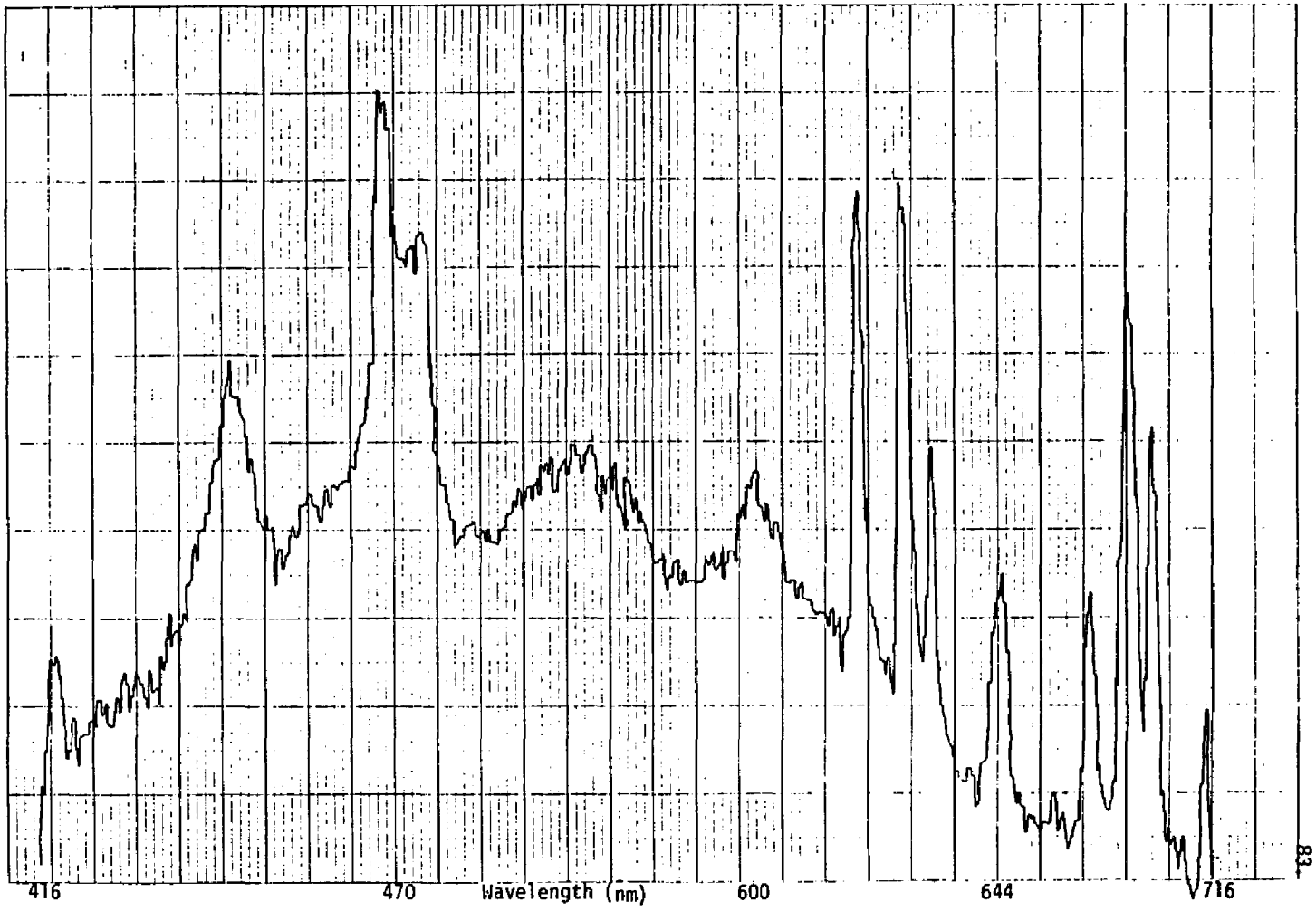

FIGURE 5 - LIDBS of CF_4

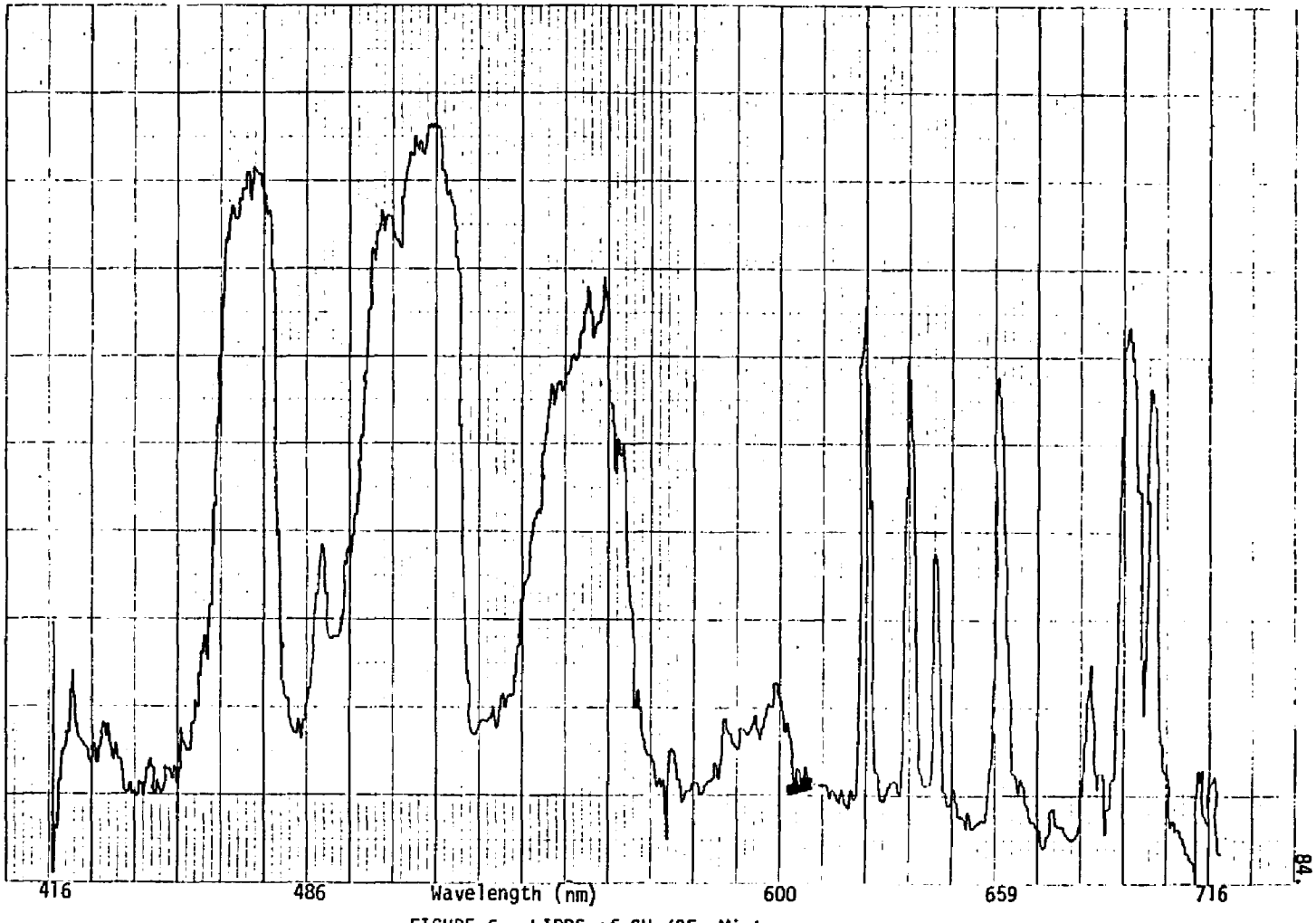

FIGURE 6 - LIDBS of CH_4/CF_4 Mixture

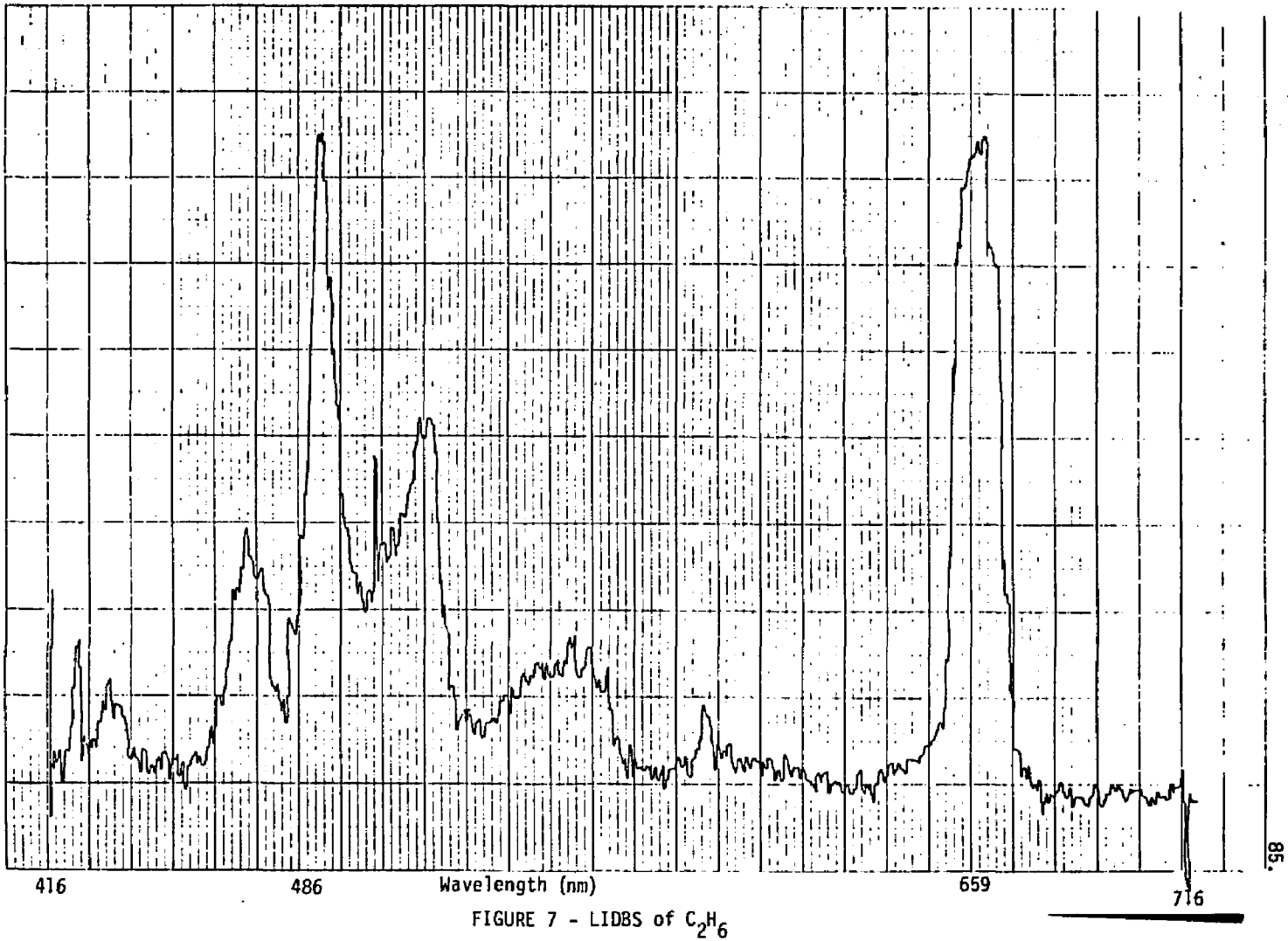

FIGURE 7 - LIDBS of C_2H_6

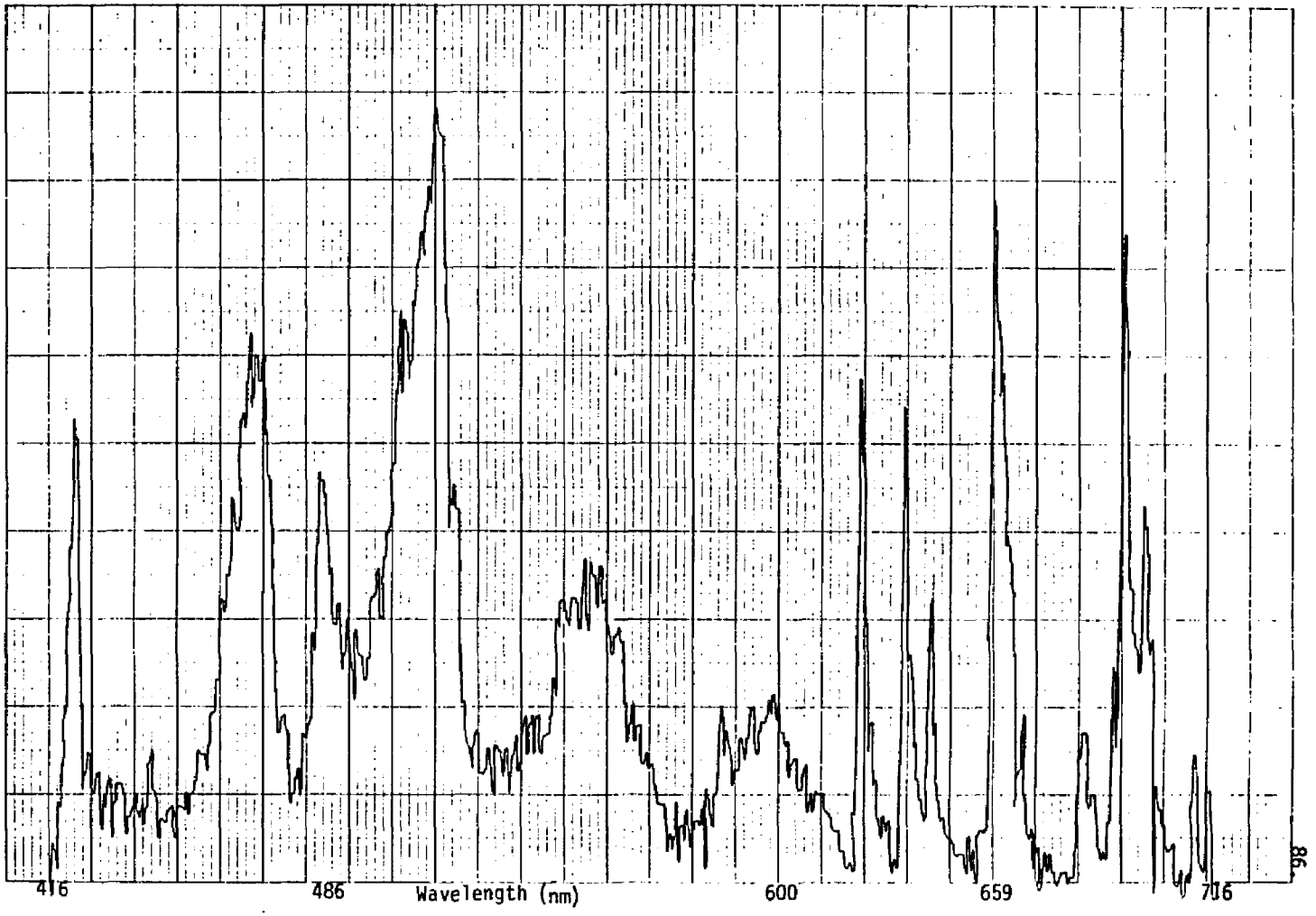

FIGURE 8 - LIDBS of C_2H_6/CF_4 Mixture

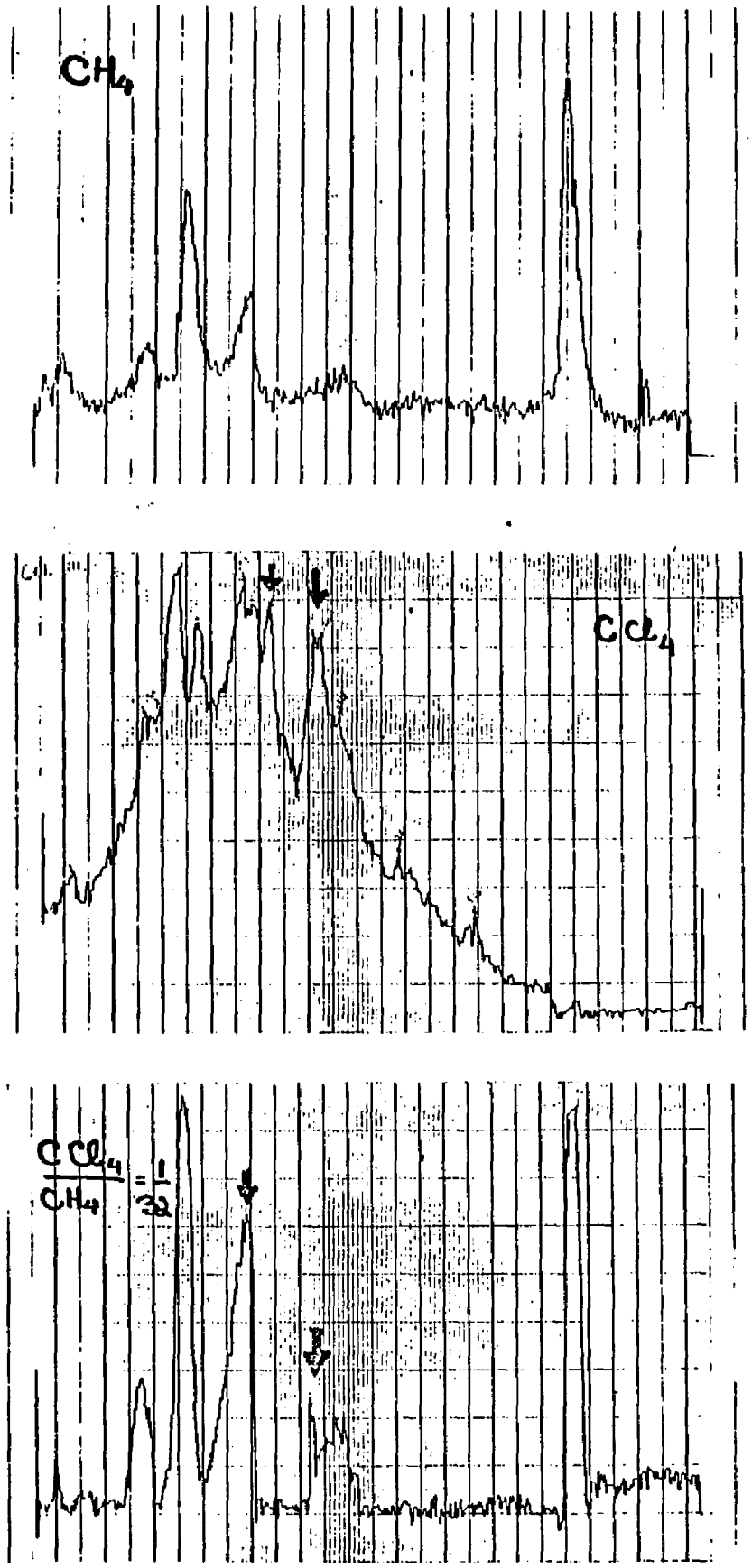

FIGURE 9

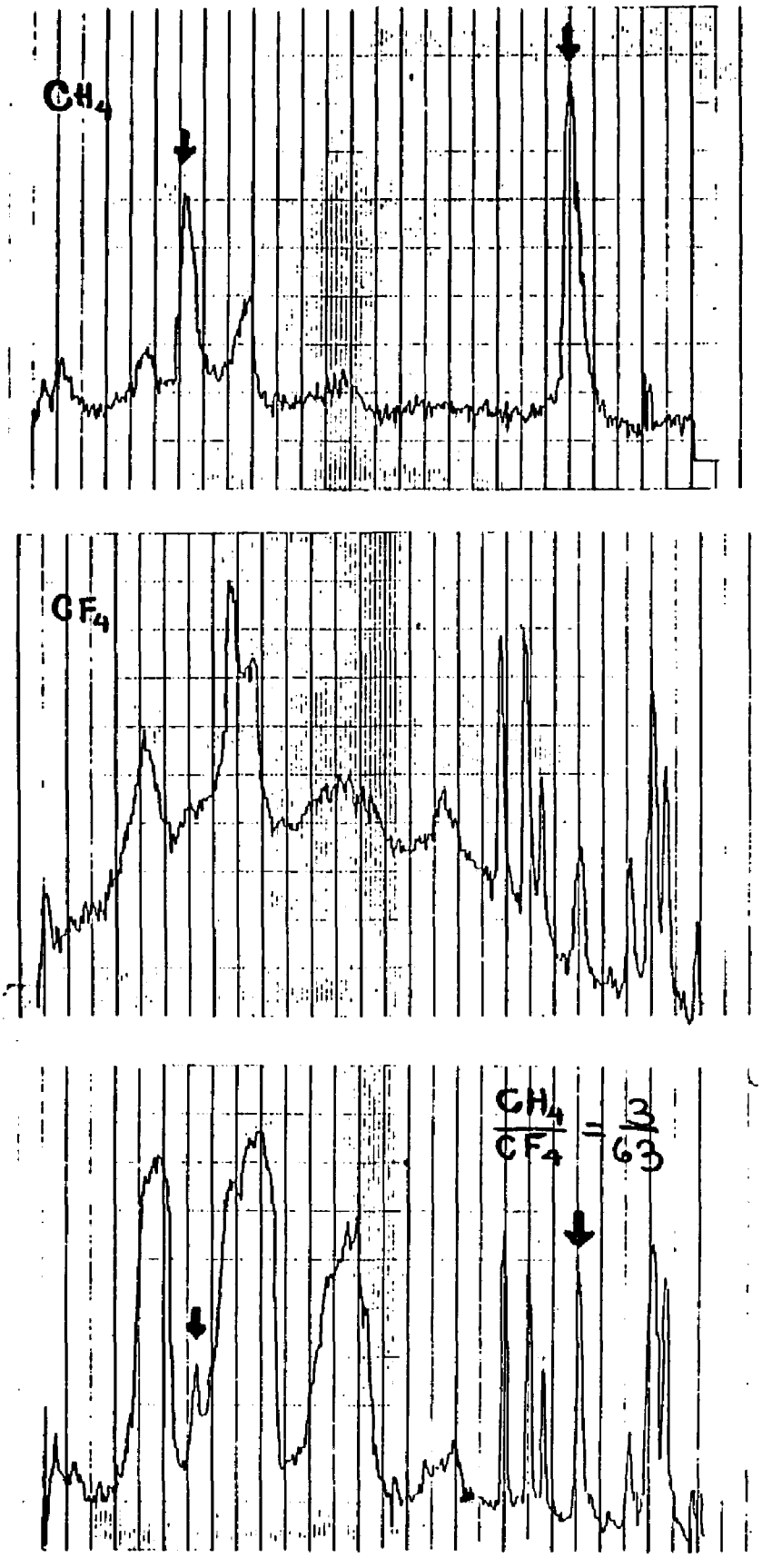

FIGURE 10

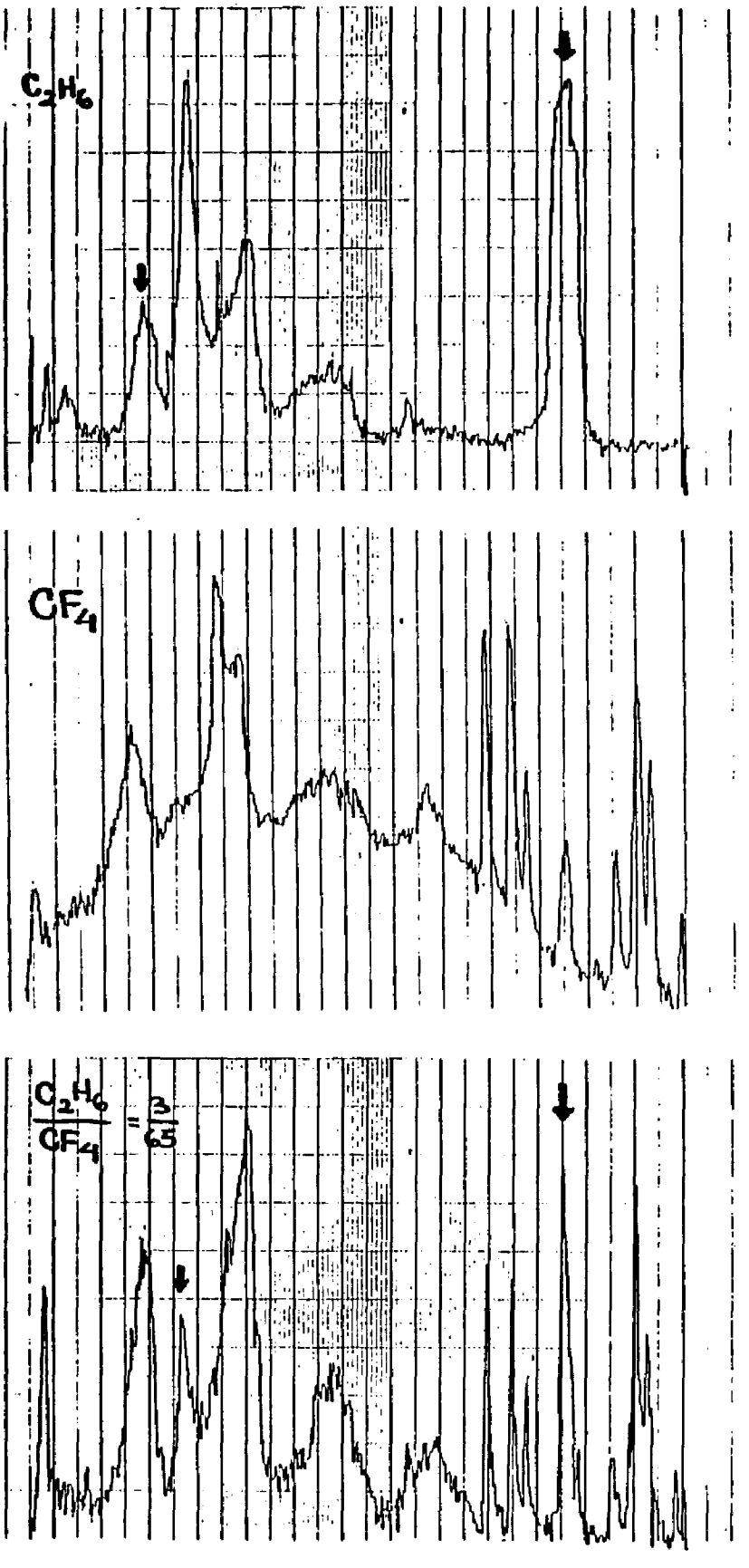

FIGURE 11

CONCULSION

The results of this study are consistent with our discussion of laser induced dielectric breakdown presented in the preceding chaper. We have seen that the technique of studying the LIDBS of different gases can have important practical applications in identifying the components of a given mixture. This technique should find particular use in probing environments which are not accessible by other methods, such as smoke stacks and atmospheric constituents near chemical plants.

Bibliography for Chapter 2

1. W. F. Meggers, C. H. Corliss, and B. F. Scribner, "Tables of Spectral Line Intensities, Part I - Arranged by Elements," NBS Monograph 145, U. S. Government Printing Office, 1975.

2. W. L. Wiese, M. W. Smith, and B. M. Glennon, "Atomic Transition Probabilities--Hydrogent Through Neon," NSRD-NBS 4, Vol. I, U. S. Government Printing Office, 1966.

3. W. L. Wiese, M. W. Smith, and B. M. Miles, "Atomic Transition Probabilities--Sodium Through Calcium," NSRDS-NBS 22, Vol. II, U. S. Government Printing Office, 1969.

4. M. W. Smith and W. L. Wiese, J. Phys. Chem. Ref. Data, 1975, 2, 85.

5. P. H. Krupenie, J. Phys. Chem. Ref. Data, 1972, 1(2), 423.

6. R. W. B. Pearse and A. G. Gaydon, "The Identification of Molecular Spectra," Wiley, New York, 1963.

7. G. Herzberg, "Molecular Spectra and Molecular Structure," Vol. III, Van Nostrand, New York, 1966.

CHAPTER 3

Laser Ignited Combustion

Introduction

The use of lasers for combustion diagnostics has received much attention in recent years[1]. Available techniques include Laser-Doppler Velocimetry (LDV) for determination of flow patterns, coherent Anti-Stokes Raman Spectroscopy (CARS) for abundant species (CH_4, O_2, N_2) and temperature determination, and Laser-Induced Fluorescence Excitation Spectroscopy (LIFES) for trace species such as free radicals (OH, CH, C_2) or polynuclear aromatic hydrocarbons (pyrene)[2]. Laser ignition, that is, using a laser to ignite a combustable mixture, has been studied sporadically through the years[3]. Many of these studies were done using visible and near infrared lasers by engineers who were interested in studying the flow pattern of the flames[4]. In this section, I will describe the systematic studies of CO_2-laser ignition on combustible mixtures ranging from hydrogen to octanewith both air and oxygen. Particular attention will be given to the limits of inflammability at sub-atmospheric pressures, spectroscopic studies of the visible and near-infrared emission of the flames and measurement of pollutant products for both "lean" and "rich" fuel mixtures.

EXPERIMENTAL

The laser apparatus was the same as described in Chapter 1. Glass cells with volumes ranging from 500 cm^3 to 1,000 cm^3 fitted with sodium chloride windows via "O"-ring joints were used in all experiments. All gases (H_2, D_2, CH_4, C_2H_4, C_2H_6, C_3H_8, O_2) were Matheson research grade and were used without further purification. Room air was used in all experiments with fuel/air mixtures. Gas pressure was measured by either a Wallace Tiernan Gauge (Model 61C-1D-0800) or a capacitance manometer (MKS Baratron). With this latter system, pressure readings could be obtained to the nearest micron. The quantitative determination of final products was carred out using an infrared spectrophotometer (Perkin Elmer 237) and gas chromatography (Hewlett-Packard 5880A). The concentration of NO_x was quantified with a mass spectrometer (Balzers QM6-511) at mass peak 30 (nitric oxide-NO). Great care was taken in this technique to correct for background mass peaks at 30 which may originate from $C^{18}O$, $^{15}N_2$, C_2H_6, and fragmentation of NO_2. The procedure was worked out carefully and calibration for each run was maintained. Additionally, some samples were sent to Gollob Analytical Services to double check accuracy.

In order to study the visible emission accompanying the explosion, an Optical Multichannel Analyzer (OMA 2) was used. This system, on loan from Princeton Applied Research Corporation, consists of a Model 1215 System Processor, Model 1216 Detector Controller, and a Model 1254 Intensified Vidicon Detector.

RESULTS

Tables I-V summarize the results of combustion mixtures of H_2/air, CH_4/air, C_2H_6/O_2, C_2H_6/air, and C_3H_8/air for pressures below one atmosphere. A cursory look at these tables reveals that laser-ignition occurs over large fuel/air ratio and total pressure ranges. One also sees that, depending on the laser conditions, i.e., power, and physical set-up, i.e., focusing, ignition may or may not take place. No real dependence was found based on cell size, with both 500 cm^3 and 1,000 cm^3 flasks used. Also, in the case of propane which has a weak absorption in the CO_2 laser region, there did not seem to be much difference if one used the laser tuned to the absorption line or if the laser was tuned "off resonance." Experiments were also done using ethylene as a fuel which has a very strong absorption in the laser region. Once again, similar results were obtained both "on" and "off" resonance though visible fluorescence[5] was observed in non-explosive "on-resonance" experiments.

The occurrence of dielectric breakdown in some mixtures raised the possibility of an electron-type mechanism as the trigger for the explosion. In order to test for that possibility, a thin slice of metal (brass, zinc, copper) was placed in the flask with the explosive mixture, and the laser beam was aimed at the metal to help create electrons in the cell. The results of these experiments are summarized in Table VI. We will return to the signifcance of these experiments in our discussion of the mechanisms of laser-ignition.

Many of the mixtures were analyzed for products. In all the hydrocarbon cases, the only products as seen from infrared spectra was CO_2 and H_2O. No nitrogen oxides or carbon monoxide was detected. An

Table I

H_2/Air Combustion

Fuel (%)	Total Pressure (torr)	Laser Power (Joules)	Focal Length	Results
3.7	202	2.8	Unfocused	Explosion
4	405	2.2	Unfocused	Explosion
4.2	405	3.3	Unfocused	Explosion
4.2	402	12	Unfocused	No Change
4.8	116	2.2	10 inches	Explosion
7.5	40	4.3	5 inches	Explosion
7.8	71	2	5 inches	Dielectric Breakdown
8.7	63	2	5 inches	Explosion
9.1	66	3	5 inches	Explosion
9.3	43	2	5 inches	Explosion
9.7	103	2	10 inches	Explosion
10	200	12	5 inches	Dielectric Breakdown
12.2	205	12	Unfocused	Explosion
15.5	71	2	5 inches	Explosion
37	80	12	10 inches	Explosion

Table II

CH_4/Air Combustion

Fuel (%)	Total Pressure (torr)	Laser Power (Joules)	Focal Length	Results
4.6	110	3	Unfocused	No Change
4.6	110	3	5 inches	Explosion
9	110	3	Unfocused	No Change
9	110	3	5 inches	Explosion
9	220	3	Unfocused	No Change
9	220	3	5 inches	Explosion
9	330	3	Unfocused	No Change
9	330	3	5 inches	Explosion
9	440	3	Unfocused	No Change
9	440	3	5 inches	Explosion

Table III

C_2H_6/O_2 Combustion

Fuel (%)	Total Pressure (torr)	Laser Power (Joules)	Focal Length	Results
9	77	1.5	5 inches	Explosion
9	165	1.5	10 inches	Explosion
13	120	1.3	10 inches	Explosion
33	27	1.3	10 inches	Dielectric Breakdown
44	90	1.3	10 inches	Explosion
50	120	1.3	10 inches	No Change
58	78	1.3	10 inches	Dielectric Breakdown
60	89	1.3	10 inches	Dielectric Breakdown
61	77	1.3	10 inches	Explosion
61	77	1.3	5 inches	No Change

Table IV

C_2H_6/Air Combustion

Fuel (%)	Total Pressure (torr)	Laser Power (Joules)	Focal Length	Results
2	125	1.6	10 inches	Dielectric Breakdown
2	184	1.6	10 inches	Explosion
2	396	10	Unfocused	No Change
2.3	191	1.7	10 inches	Dielectric Breakdown
2.5	200	1.7	5 inches	Dielectric Breakdown
3	206	1.7	10 inches	Explosion
3	196	1.9	10 inches	Explosion
3.2	100	1.8	10 inches	Explosion
3.2	50	1.8	10 inches	Dielectric Breakdown
3.3	97	1.9	10 inches	Explosion
3.3	180	10	Unfocused	No Change
3.3	180	10	5 inches	Explosion
3.4	50	1.8	10 inches	Explosion
3.5	100	1.8	10 inches	Explosion
3.5	100	1.9	10 inches	Explosion
3.5	100	10	Unfocused	No Change
3.5	100	10	5 inches	Explosion
3.7	95	1.8	10 inches	Explosion
3.7	94	1.8	10 inches	Explosion
4	187	1.7	10 inches	Explosion
4.5	200	1.7	10 inches	Explosion
5	200	10	Unfocused	No Change
5	200	10	5 inches	Explosion
5	390	10	Unfocused	No Change
5	390	10	5 inches	Dielectric Breakdown
7	97	1.6	10 inches	Dielectric Breakdown
7.5	390	10	5 inches	Dielectric Breakdown

Table V

C_3H_8/Air Combustion

Fuel (%)	Total Pressure (torr)	Laser Power (Joules)	Focal Length	Results
1.1	100	1.8	10 inches	Dielectric Breakdown
2.5	100	1.6	10 inches	Explosion
3	100	1.8	10 inches	Explosion
3	102	2.1	10 inches	Explosion
3.1	103	1.2	10 inches	Explosion
3.2	100	1.5	10 inches	Explosion
3.3	108	1.8	10 inches	Explosion
3.4	105	1.1	10 inches	Explosion
3.7	100	1.8	10 inches	Explosion
4	100	1.6	10 inches	Explosion
6.2	192	1.5	10 inches	Explosion
8	200	1.7	10 inches	Dielectric Breakdown

Table VI

C_2H_6/Air Unfocused With Brass Metal

Fuel (%)	Total Pressure (torr)	Results
1	55	Dielectric Breakdown
3.3	55	Explosion
5	52	Dielectric Breakdown
5	99	Explosion
6	102	Explosion
7	101	Explosion
8.2	101	Dielectric Breakdown

infrared spectrum of a C_3H_8/air mixture is shown in Figure 1 for both before and after combustion. Mass spectral analysis was done on a series of CH_4/air mixtures for "lean," "rich," and stoichiometric mixtures. The results are summarized in Table VII. As a comparison to laser ignition, combustible mixtures were also ignited using a spark plug (Champion L76V) in conjunction with a battery, coil, and a switch. Table VIII gives the results of spark emission for CH_4/air mixtures. In comparing the results of laser and spark ignition, one sees that the results are similar with only one notable difference. In all cases, the laser-ignition concentration of NO_x is lower than that of the spark combustion.

The intense light that accompanied the combustion was studied using the OMA-2 system. In all mixtures, there was a very intense peak at 588 nm and, for the hydrocarbon fuel mixtures, there was another peak further to the blue at 431 nm. The intensity of the "blue" peak seemed to be governed by the number of carbons in the hydrocarbon, increasing with additional carbons. Figures 2-5 show the visible emission spectrum of the different mixtures studied. Since the peak at 588 nm was the dominant one in the spectrum, its identification is of prime importance. Both H_2/air and H_2/O_2 mixtures gave the same emission proving that the peak was not due to N_2, NO, NO_2, etc. In order to test for the possibility of its being HO_2, a mixture of deuterium and oxygen was ignited. This spectrum is shown in Figure 6. The emission is not at all shifted from the H_2/O_2 mixture precluding the possibility of the peak being due to hydrogen alone or a hydrogen-oxygen species. We, therefore, concluded that the emission at 588 nm is probably due to ozone[11].

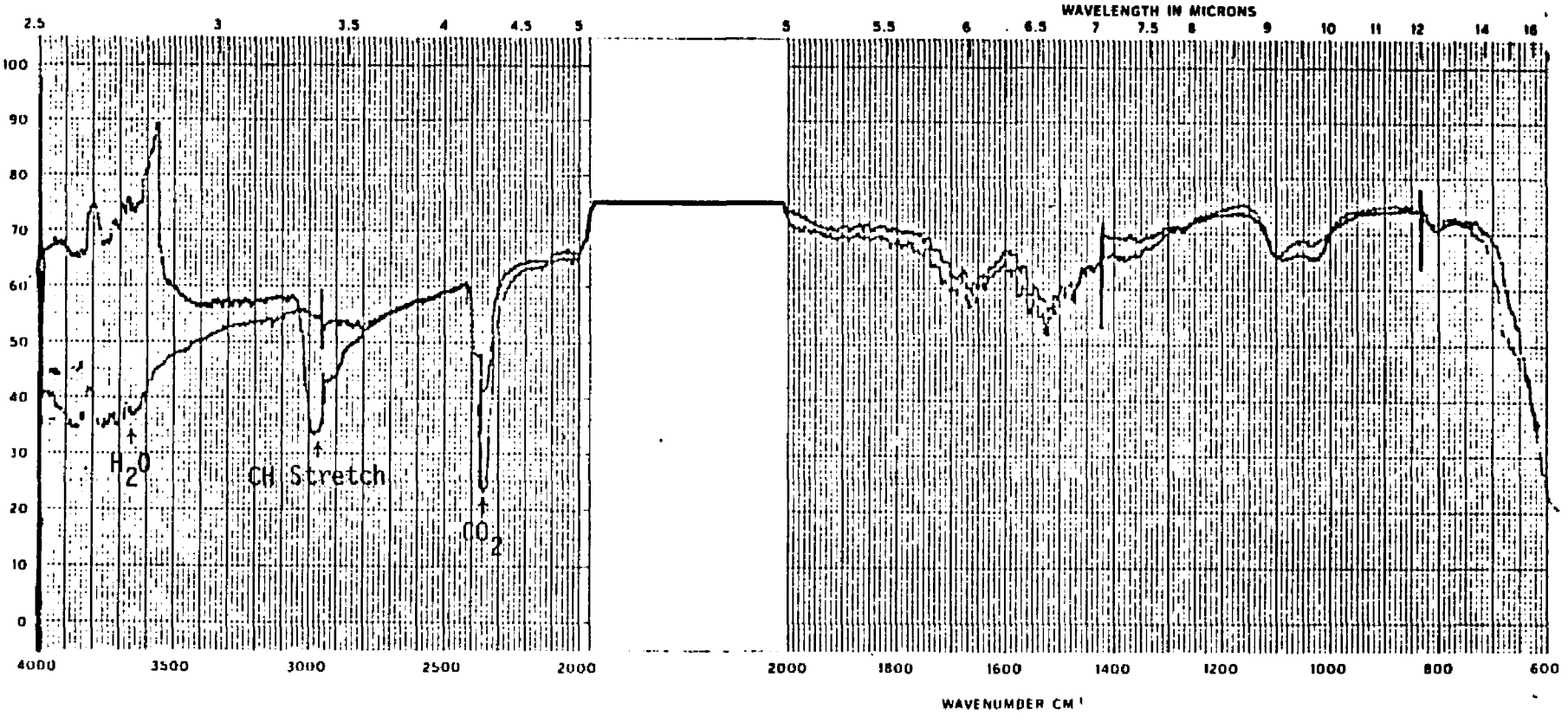

FIGURE 1

IR Spectrum C_3H_8/Air Before (Top Trace) and After Combustion (Lower Trace)

Table VII

CH_4/Air

One Atmosphere Total Pressure

Laser Ignition

Initial Sample Concentration	Final Sample Composition[a]				
CH_4/Air	CO_2	CO	CH_4	C_2H_6	NO_x
8.6%	9.6	0.2	0.2	ND[b]	0.005
9.5%	9.8	0.3	0.2	ND[b]	0.005
10.5%	7.3	5.0	0.17	ND[b]	< 0.005

[a] Analyzed using Gas Chromatography and Mass Spectroscopy. Each sample represents the average of at least 5 runs.

[b] Not detected; less than 50 ppm.

Table VIII

CH_4/Air

One Atmosphere Total Pressure

Spark Ignition

Initial Sample Concentration	Final Sample Composition[a]				
CH_4/Air	CO_2	CO	CH_4	C_2H_6	NO_x
8.6%	9.1	ND[b]	0.11	ND[b]	0.027
9.5%	10.4	ND[b]	0.13	ND[b]	0.091
10.5%	8.9	2.6	0.12	ND[b]	0.017

[a] Analyzed using Gas Chromatography and Mass Spectroscopy. Each sample represents the average of at least 5 runs.

[b] Not detected; less than 50 ppm.

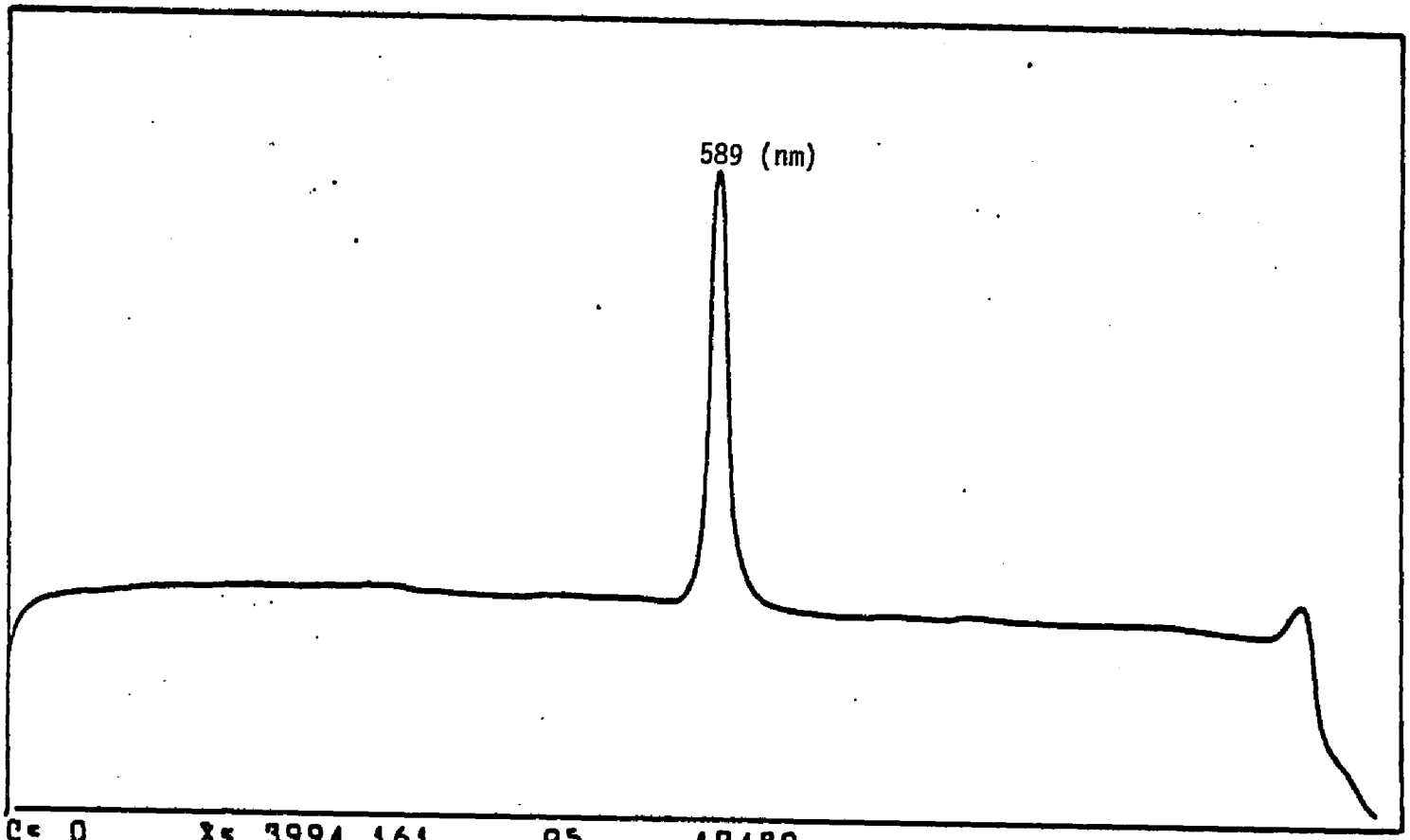

FIGURE 2

OMA Spectrograph of H_2/Air Combustion

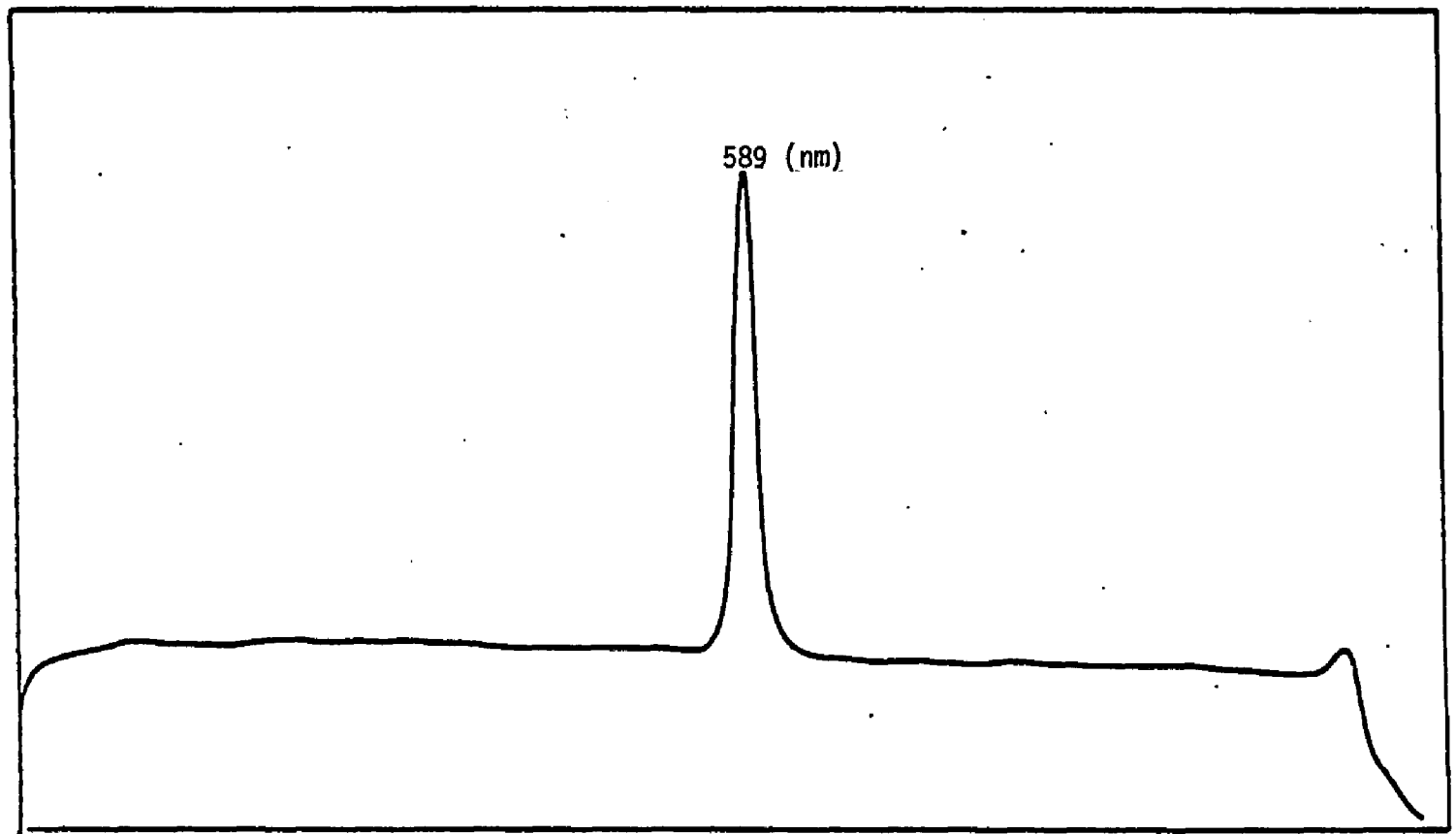

FIGURE 3

OMA Spectrograph of C_2H_6/Air Combustion

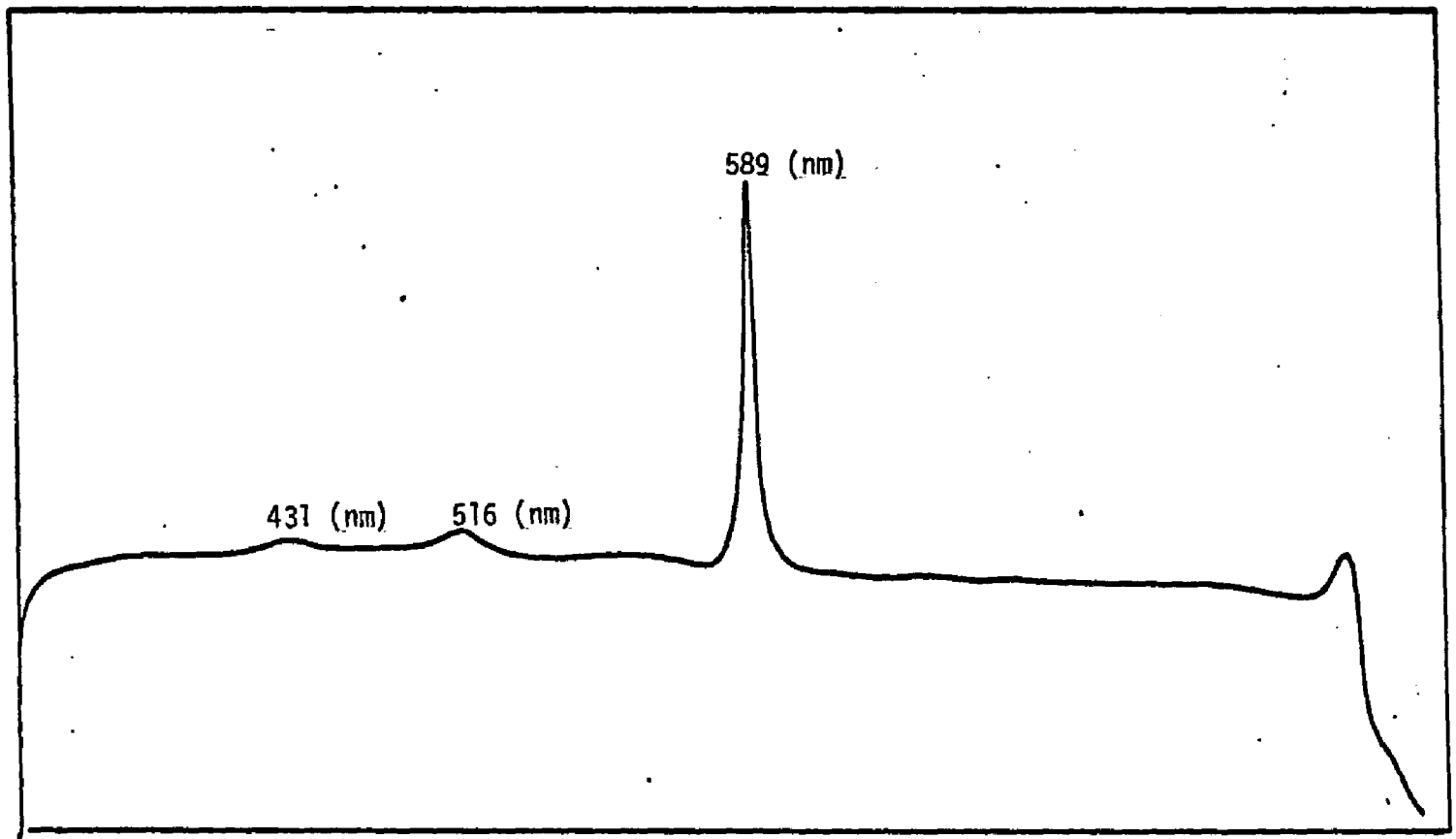


```
C= 0      X= 3994.161      18      15497
TIMING 1                  SCAN MODE  1          COMP MODE  0
X0  0       CHNLS  500     DATA/TRK  500        US/CHNL  60
Y0  100     DELTY  400       TRACKS  1          MS/TRK  30.000
      DELAY  100E-6        WIDTH  100E-6   SINGLE? 1
FULL SCALE  0             @ CHNL  0              HEAD  1
PREP SCANS  15             SCANS  200            TIME  15:538
D18:  YSPIDIT 10 INCH CC ORANGE BLUE 17
```

FIGURE 4

OMA Spectrograph of C_3H_8/Air Combustion

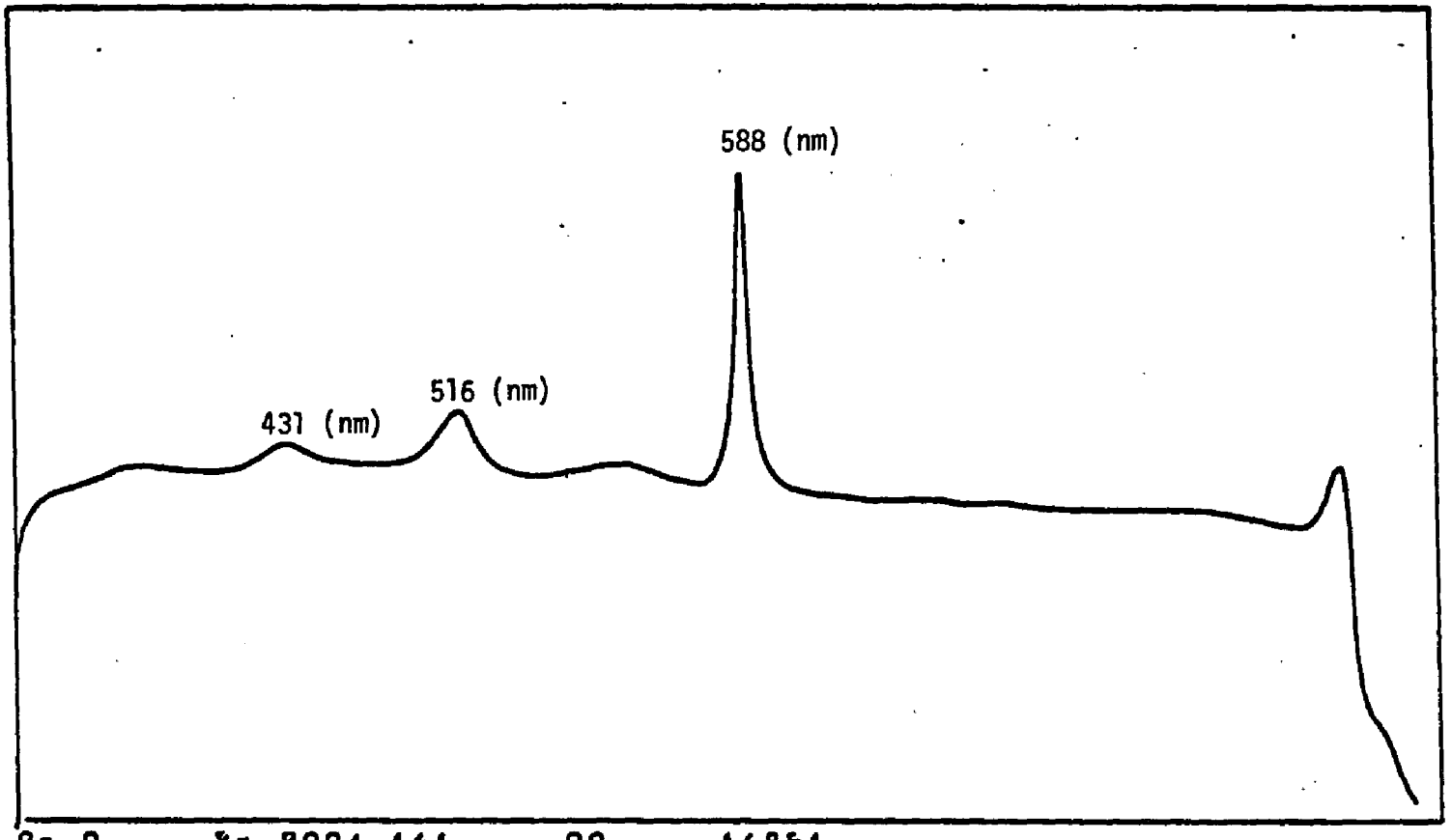

C< 0 X< 3994.161 29 16851
TIMING 1 SCAN MODE 1 COMP MODE 0
XD 0 CHNLS 500 DATA/TRK 500 US/CHNL 60
YD 100 DELTY 400 TRACKS 1 MS/TRK 30.000
DELAY 100E-6 WIDTH 100E-6 SINGLE? 1
FULL SCALE 0 @ CHNL 0 HEAD 1
RECP SCANS 15 SCANS 200 TIME 85:455
029: Y2.50CT105T CE 18

FIGURE 5

OMA Spectrograph of C_8H_{18}/Air Combustion

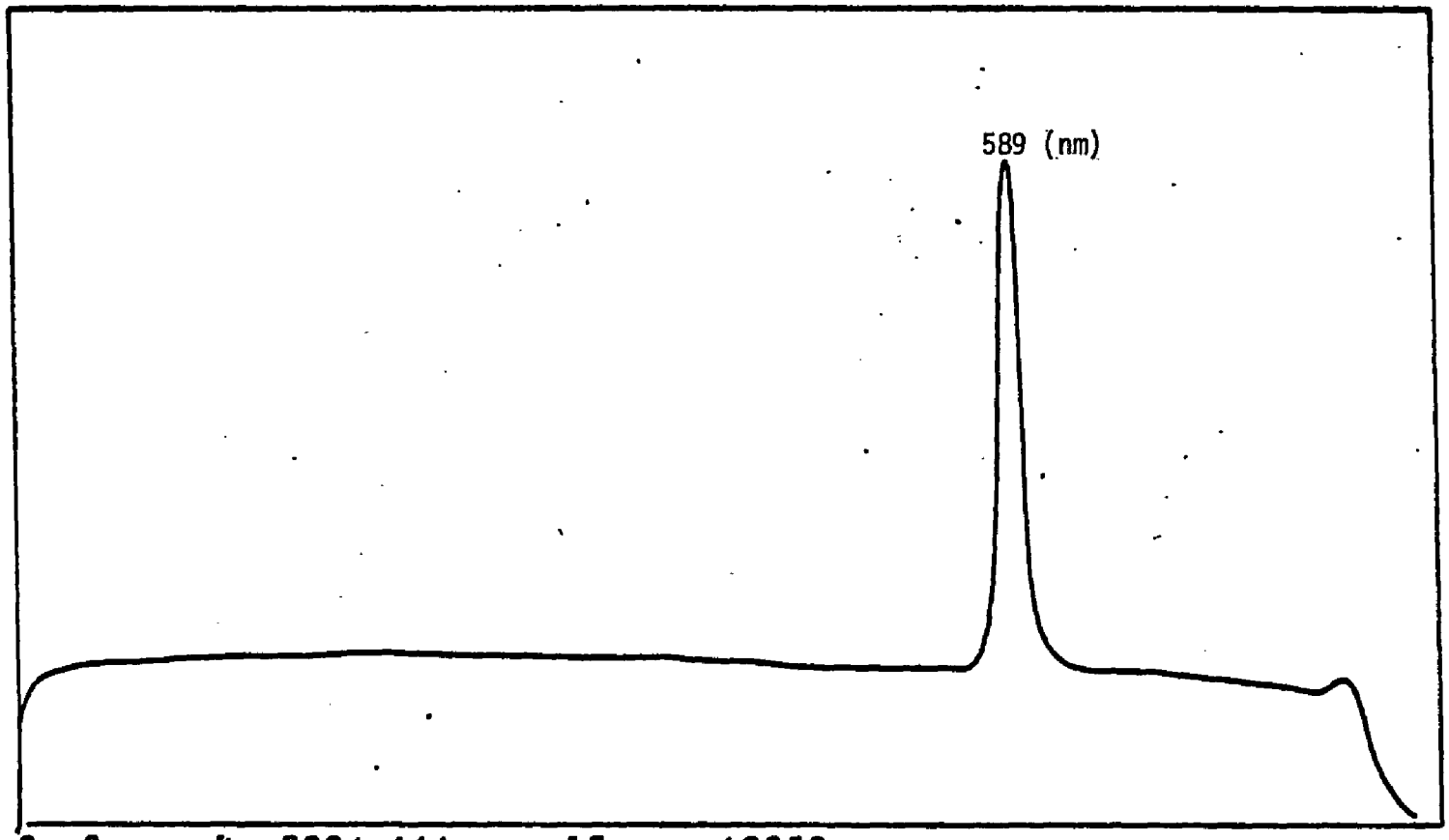

FIGURE 6

DHA Spectrograph of D_2/Air Combustion

The emission at 4314 Å is probably due to CH radicals found during ignition and, therefore, it increases in intensity as the number of carbons and hydrogens are increased.

The peak at 516 nm can be attributed to C_2 radicals which should also increase in intensity as the number of carbons are increased.

DISCUSSION

From the point of view of their technological and economical position in our industralized society, the oxidation reaction of hydrocarbons are of prime importance. Parallel to the utility of these reactions and other associated chain reactions is their chemical complexity and the multitude of unique phenomena associated with their kinetic behavior.

Few reactions have been studied as extensively as the classical reaction of hydrogen and oxygen[6]. This reaction, due to its relative chemical simplicity, has served as a prototype and proving ground for theories of branching chain explosions. To summarize, the results of H_2/O_2 reaction show that, in the range of 400° to 600°C, there is a branching chain explosion replete with three explosion limits. Table IX summarizes the thermodynamic data for the species known to exist in a reacting mixture of H_2 and O_2 in temperature range 400° to 600°C. The simplest kinetic scheme which can be used to account for both the explosion limits and the stationary-state reaction is the following:

Initiation	$H_2 + \text{wall} \rightarrow W{\cdot}H + H$	
Propogation:	$H + O_2 \rightarrow HO + O$	-15.3 kcal
	$O + H_2 \rightarrow HO + H$	+1 kcal
	$HO + H_2 \rightleftarrows HOH + H$	+13.8 kcal
Chain Transfer:	$H + O_2 + M \rightarrow HO_2 + M$	+40 kcal
Termination:	$H + \text{wall} \rightarrow$ stable species	
	$HO_2 + \text{wall} \rightarrow$ stable species	
	$HO + \text{wall} \rightarrow$ stable species	

Table IX

Thermodynamic Data For Species of Importance in the System

$2H_2 + O_2 \rightarrow 2H_2O$ (Gas Phase)

Species	H_f° (kcal/mole)	S_p° (cal/mole·K)	C_p° (cal/mole·K)
H_2	0.00	31.2	4.97
O_2	0.00	49.0	7.02
H_2O	-57.8	45.1	8.03
H_2O_2	-31.8	54	8.5
O_3	34.0	56.8	9.12
H	52.1	27.4	4.97
O	59.2	38.5	5.24
HO	8.0	43.9	7.14
HO_2	12	56	8.5

Data from National Bureau of Standards, Circ. 500

The stable species referred to in the termination reactions are presumed to arise from the reactions of the atoms and free radicals with similar species already absorbed at the wall. Thus, if H atoms are adsorbed on active sites on the wall, they can produce H_2 with more H atoms or H_2O with OH or $H_2 + O_2$ from HO_2.

Hydrocarbon oxidations are considerably more complex than its hydrogen counterpart due in part to the fact that free radicals can catalyze the cracking reaction of hydrocarbons. Although there is no direct information on the method of initiation of radicals in the combustion reaction, there seems to be fairly general agreement on the reaction

$$RH + O_2 \rightarrow R + HO_2$$

i.e., an abstraction of an H atom.

Given the preceding discussion, it is reasonable to assume that laser-ignition should at least initially undergo a similar mechanism as thermal explosion. That is, one would expect that the energy of the laser can strip a hydrogen atom from the hydrocarbon to initiate the combustion. However, it is not perfectly clear as to how the output of the laser can achieve this result given that, in the many cases we studied, there was no resonant absorption of the laser energy since the gases involved did not have an infrared vibrational frequency that matched the CO_2 laser frequency.

In order to explain this phenomenon, we must review shortly some of the ideas of laser induced dielectric breakdown discussed in the previous chapters. For many years, it has been known that the focused

output of a laser can induce a spark in gases. The plasma formed has been found to be rich in ionic, neutral, and radical species dependent on the gas studied. The accepted theoretical explanation of the formation of this plasma is that an exoelectron is accelerated by the laser via inverse Brehmsstralung and then via an avalanche-type effect producing a critical electron density which can ionize the gas. This effect allows the use of laser chemistry even in gases where there is no resonant absorption. Extensive studies on a variety of gases have shown that each gas is ionized at a given pressure for a given laser power. Though no one factor can be singled out as the reason for plasma formation, a study of a series of fluoromethanes has shown that the pressure for achieving dielectric breakdown at a given power seems to correlate fairly well with the ionization potential of the molecule[7]. With this in mind, I will now proceed to discuss what I believe to be the mechanism of laser ignition.

Using C_2H_6/air mixtures as an example and by referring to Table IV, we note that laser ignition can be achieved in the range of 3% to 8% fuel content at a total pressure of 100-300 torr. At lower fuel ratios, there was often no reaction while, above those ratios, there was only dielectric breakdown without combustion. The explanation of these observations is that, in order to have ignition, a sufficient number of hydrogen atoms must be formed to initiate the chain reactions. The H atoms are formed via the usual dielectric breakdown in the gas mixture. After the H atom formation, the usual chain reaction takes place. Below the critical fuel pressure, we do not form enough H atoms to initiate the chain. Since the laser output interacts with both the fuel and air in the mixture, increasing the total pressure does not

significantly decrease the explosion limits.

The difficulty in using the above explanation for the ignition mechanism lies in the fact that, above a certain fuel ratio, ignition is inhibited and only dielectric breakdown occurs. One might expect that, by increasing the hydrocarbon content, one increases H atom production which should make for more efficient combustion. To explain this discrepancy, we must remember that we are not only producing more H atoms but other ionic, neutral, and radical species as well. In fact, the production of these other species will actually hinder the combustion process rather than help it. Furthermore, this situation is exactly the same as that found in conventional spark ignition as shown in Table X.

Further proof of this explanation can be seen by the fact that, at certain pressures, laser combustion was achieved by focusing with a 10" lens but not with a 5" lens. By using a 10" lens, we have a "softer" focusing situation where we have milder conditions with the plasma. Therefore, we do not inhibit the explosive reaction. On the other hand, with a 5" lens, the conditions are more severe and we may, in fact, produce too many ionic species which inhibit the combustion reaction and instead we obtain a typical dielectric breakdown.

In order to prove further that laser ignition is initiated via an electron spark mechanism similar to dielectric breakdown, experiments were done using the laser in an unfocused configuration. In all cases, in order to initiate dielectric breakdown in a gas, the laser must be focused. The reason for this is because, without focusing, the electron density is not large enough to intiate plasma formation. Even for the case of iron carbonyl, which has one of the lowest thresholds for

Table X

Limits of Inflammability[a]

Compound	Lower Limit	Upper Limit
CH_4	5.00	15.00
C_2H_6	3.00	12.50
C_3H_8	2.12	9.35
C_4H_{10}	1.86	8.41
C_5H_{12}	1.40	7.80

[a] All limits at atmospheric pressure and room temperature for upward propagation in a tube or bomb 2 inches or more in diameter. Values are on a percentage by volume basis.

Taken from U. S. Bureau Mines Tech. Paper No. 544, 1933.

breakdown[8], an unfocused beam will not initiate breakdown even at elevated pressures. Similar results were found in our study of laser ignition. A cursory glance at Tables I-V shows that, without focusing, we were unable to initiate combustion. In those cases where the beam was not perfectly aligned and it was allowed to strike the surface of the cell, there was successful ignition in certain instances. This too is consistent with our notion, for it is known that impurities in the cell are easily ionized which can lead to the spark necessary for ignition[9]. Furthermore, when a thin slice of metal was placed in the cell and the beam was passed across it, ignition was observed without focusing. The metal served to provide a convenient source of electrons which, when accelerated by the beam, produced the necessary avalanche to initiate the spark.

The above discussion seems to clearly show that laser ignition proceeds via a dielectric breakdown type mechanism. In fact, laser combustion is a direct extension of dielectric breakdown applied to a combustible mixture. We shall now turn our discussion towards the other interesting aspects of laser ignition, namely the combustible limits, product formation, and visible spectroscopic studies.

One of the more interesting findings in our study on laser ignition revolves around the air-to-fuel ratio (A/F) necessary for successful combustion. A typical automobile engine having a standard spark ignition system is usually run at an A/F ratio of 15:1[4]. In fact, above ratios of 22:1, spark ignition will not occur. By contrast, our studies indicate that laser ignition is successful even at ratios as large a 33:1. This extension of the laser limit of operation can be attributed to the higher spark energy of the laser. The total energy

output of the laser was between 1 and 2 Joules with a peak power of approximately 1 megaWatt in about 1 microsecond. The fact that our pulse duration is about 1/1000 the duration of a standard spark also should allow for a more rapid pressure rise for the laser system. Indeed, pressure rise measurements done on a series of CH_4/air combustions show that, in all cases, the risetime of the laser ignited signal is significantly faster than spark ignition. Also, the onset of the pressure wave comes more quickly and the maxima achieved is much higher for laser ignition. It was also found that, by increasing the fluence of the laser, even stronger maxima can be attained. These findings of a higher and more rapid rise in pressure using the laser should lead to a better performance of an engine and also, obviously, allows for greater overall fuel economy.

In our industrialized society, we have come to expect that new technology often leads to serious environmental problems. On of the greatest of these problems involves the exhausting of pollutants such as carbon monoxide (CO), hydrocarbon (HC), and nitrogen oxides (NO_x) by automobile engines. In the case of nitrogen oxides, a search of the available literature fails to explain why normally nonreactive N_2 manages, with no known catalyst, to combine with O_2 to form the oxide on the order of several hundred ppm. As is often the case, we must accept the experimental findings and try to improve on them even though there is no sound theoretical base for these findings. I shall now summarize some of the fundamentals and then describe how industry is trying to cope with emission standards.

Emissions within the engine are formed when the hydrocarbon fuel is burned incompletely to HC and CO in the engine's combustion chamber.

Ideally, the fuel and oxygen in the air entering the chamber yield harmless exhaust products, i.e., carbon dioxide, water vapor, and inert nitrogen. But the generation of the pollutants, CO, HC, and NO_x (mainly NO), is a function of the relative amounts of air and fuel. At high air-fuel (A/F) ratio, CO and HC emission are decreased because of the greater quantity of oxygen available for combustion. NO_x, on the other hand, is an exponential function of flame temperature. At low temperature, nitrogen and oxygen from the air will not unite to form significant concentrations of NO. Low temperature is achieved at A/F mixtures richer and leaner than the optimum because of the effect exerted by unburned fuel in the former case and the excess air in the latter. Optimum burning within the engine, which is closer to the stoichiometric point, results in the greatest concentration of NO_x formed (Figure 7). In order to control the emission of HC and CO, high exhaust gas temperatures are needed. However, lower exhaust temperatures would increase fuel economy and decrease NO_x production. To resolve these perplexing problems, different devices such as catalytic converters and exhaust gas recirculation (EGR) systems came into being. These devices try to control exhaust pollutants by converting them to harmless products and lower peak combustion temperature by use of inert gases. These technological advances in turn caused a host of other problems. Some of these include the poisoning of catalytic converters by leaded gasoline, the oxidation of sulfur to sulfur dioxide and eventually to sulfuric acid and the possible toxicity of some of the catalysts themselves to name but a few[10].

I believe that our preliminary results on the use of a laser for combustion initiation should lead to a greater interest in the use of the laser as a combustion tool. Our results indicate that laser

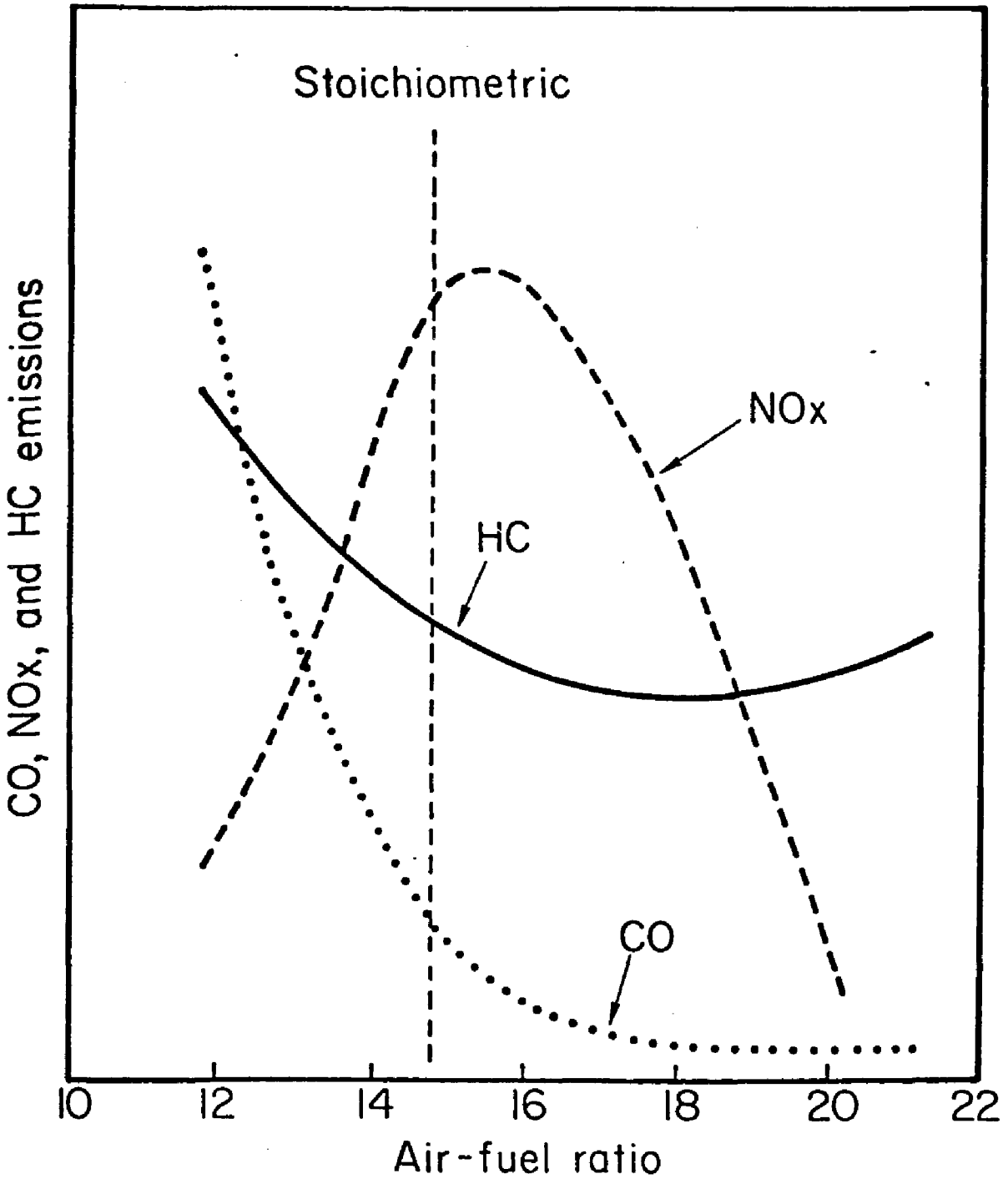

FIGURE 7

Effect of Air-Fuel Ration on Exhaust Composition

ignition can be achieved in leaner mixtures than conventional sparks which can lead to better fuel economy. Moreover, our experiments seem to indicate that laser combustion results in lower NO_x formation than spark ignition. This finding can possibly be explained by remembering that the intense laser energy is deposited in the sample in less than a microsecond which may not allow significant amounts of NO_x to be formed. By contrast, the sparks used in combustion are on the order of several milliseconds. It is possible that, with the advent of even shorter laser pulses on the order of picoseconds, even less NO_x may be formed. Also, by using leaner mixtures, more complete combustion can be obtained thereby reducing the amounts of HC emissions. On the other hand, there are also some obvious drawbacks to the use of lasers in combustion. One of these would be the power consumption necessary to drive an engine. Assuming that 0.5 Joules/pulse is consumed for ignition, a laser ignition system for a 6 cylinder engine running at 2400 rpm uses about 60 W of pulsed laser power. Generating this power with a system of 10% efficiency would require 600 Watts or about 8 horsepower. However, with the continuing advances in laser technology, this power consumption may be reduced.

Finally, we shall now turn to the spectroscopic studies of the transient species produced during ignition. As described earlier, these studies were done using the OMA system, allowing for complete identification of visible emissions with one laser pulse. Unfortunately, these spectra were not as rich as one mighthave hoped. The intense visible light accompanying the combustion only gave rise to the two major peaks in the spectra. The CH radicals formed are consistent with the formation of such radicals in the dielectric breakdown of any

number of hydrocarbon species. In contrast to the dielectric breakdown of hydrocarbons, the combustion did not show any visible emission from atomic species either neutral or charged. In the previous chapter, we summarized the emission spectra of many molecules after dielectric breakdown also using the OMA system. As one can see, the emission spectrum is much cleaner in the combustion case than in typical breakdown.

The peak at 588 nm is quite perplexing and seems to elude identification. At best, we can conclude that it is probably ozone which has a band at that wavelength[11] or possibly HO_2. Regardless, the rise and fall time of this peak does not differ considerably from the typical signal of a high pressure luminescence which often accompanies CO_2 laser dissociation.

Recently, researchers have turned to infrared fluorescence as a tool in the study of simple chain reactions. Nesbitt and Leone[12] have used this technique in the study of H_2/Cl_2 chain reactions and other hydrocarbon/Cl_2 chains. Their reactions are carried out under much more controlled conditions and they purposely avoid outright explosion. By varying the pressure and studying the rise and fall of the infrared fluorescence, important information is obtained regarding the transients in these complex reactions. When we tried to apply this technique to combustion reactions using an InSb detector, the signal was so intense that the detector was completely saturated. We also tried to look for luminescence at 1.6 microns in the near infrared using a Ge detector. At this wavelength, HO_2 is expected to emit. However, in our combustion studies, no luminescence was detected at this wavelength. In conclusion, the spectroscopic studies of combustion show that CH radicals, O_3, and possible HO_2 radicals are formed in the process.

These radicals are expected to play an important role in combustion processes but no particular dependence was found on the hydrocarbon or pressure used in the formation of these transients.

CONCLUSION

The combustion studies reported here have established some information about laser ignition, namely, that the laser will readily ignite a range of combustible mixtures, that the laser will ignite lean mixtures, that the laser may give lower NO_x concentrations, and that the laser gives rise to a more rapid flame speed.

Interest in the laser as a tool in combustion studies will be greatly facilitated as new laser systems become available where the energy per pulse required for breakdown is significantly reduced. Also, shorter laser pulses and better focusing systems should also lead to the greater uses of lasers in the combustion field.

Bibliography for Chapter 3

1. A. C. Eckbreth, P. A. Boncyzk, and J. F. Verdieck, Appl. Spectrosc. Revs., 1978, 13, 15.

2. D. S. Coe and J. I. Steinfeld, Proc. Symp. on Laser Diagnostics for Combustion Processes, A.C.S. National Meeting, Wash., D. C., 1979.

3. G. G. Bach, R. Knystautas, and J. H. Lee, 12th International Symp. on Combustion, 1969, 853.

4. J. H. Dale, P. R. Smy, D. Way-Nee, and R. M. Clements, Combustion & Flame, 1977, 30, 319.

5. J. H. Hall, M. L. Lesiecki, and W. A. Guillory, J. Chem. Phys., 1978, 68, 2247.

6. N. Semenoff, "Chemical Kinetics and Chain Reactions," Clarendon Press, Oxford, 1935.

7. S. T. Lin, Ph.D. Dissertation, City University of New York, 1978.

8. Y. Langsam, Ph.D. Disseration, Polytechnic Institute of New York, 1979.

9. J. Black and E. Yablonovitch, IEEE, J. Quant. Electron, 1977, QE-13, 117.

10. L. Gibney, Environmental Science & Technology, 1974, Vol. 8, No. 9, 793.

11. G. Herzberg, "Molecular Spectra and Molecular Structure," Vol. III, 1966.

12. D. Nesbitt and S. R. Leone, SPIE Proc., 1978, 158, 29.